Journal of Materials Chemistry B

ROYAL SOCIETY OF CHEMISTRY

REVIEW

View Article Online
View Journal | View Issue

Cite this: *J. Mater. Chem. B*, 2022, **10**, 7418

Molecularly imprinted polymers in diagnostics: accessing analytes in biofluids

Yasemin L. Mustafa, [ab] Antonios Keirouz [ab] and Hannah S. Leese *[ab]

Bio-applied molecularly imprinted polymers (MIPs) are biomimetic materials with tailor-made synthetic recognition sites, mimicking biological counterparts known for their sensitive and selective analyte detection. MIPs, specifically designed for biomarker analysis within biofluids, have the potential to significantly aid patient diagnostics at the point-of-care, enabling self-health monitoring and management. Recent research in this field, facilitated by the hybridisation of materials science and biology, has developed and utilised a variety of different polymerisation synthesis methods tailored to the bio-application of MIPs. This review evaluates the principles of molecular imprinting for disease diagnostics, including recent progress in integrated MIP-sensor technologies for high-affinity analyte detection in complex biofluids from serum and saliva to cerebrospinal fluid, sweat, urine, nasopharyngeal fluid, and tears. The work highlights the state-of-the-art in the progression of MIP-sensor technologies' translation into commercially available sensors and their potential contribution to disease detection systems in healthcare settings.

Received 30th March 2022,
Accepted 20th June 2022

DOI: 10.1039/d2tb00703g

rsc.li/materials-b

[a] *Materials for Health Lab, Department of Chemical Engineering, University of Bath, Bath, BA2 7AY, UK. E-mail: h.s.leese@bath.ac.uk*
[b] *Centre for Biosensors, Bioelectronics and Biodevices (C3Bio), University of Bath, Bath, BA2 7AY, UK*

Hannah S. Leese

Hannah S. Leese is assistant professor in the Department of Chemical Engineering at the University of Bath. She received her Ph.D. in Chemical Engineering (2013) and held post-doctoral research associate positions at Imperial College London (2013–2017) and the University of Manchester (2017–2018). Together, Hannah's team, the Materials for Health Lab, engineer advanced materials for minimally invasive point-of-care diagnostics for the early detection of disease – including molecularly imprinted polymers as sensor elements in devices, hydrogel-based microneedle technologies for drug delivery and biomarker uptake, devices for early detection of ovarian cancer and biomimetic protein-based fibres for wound dressing textiles.

Introduction

Until recently, medical diagnostics have primarily relied on laboratory verification, often providing delayed results due to laborious processes, in addition to requiring specialised equipment and medically trained personnel.[1–3] However, the rising demand for medical testing devices at the point-of-care, combined with the continuous interconnecting of medicine and digital technologies, has facilitated the fabrication of devices with high selectivity, specificity, and rapid response times.[4] The evolvement of such devices has been internationally recognised as a focal point during the COVID-19 pandemic, highlighting further, the urgent call to advance accurate, rapid, and reliable medical diagnosis and treatment.[5–9]

Point-of-care devices can negate issues associated with current clinical instruments, instead, offering fast results, small sample volumes, easy transportability, and minimal technical training. Commercially available point-of-care biosensors, such as the FreeStyle Libre 2 (Abbott, USA), Accutrend® Plus system (Roche, Switzerland), and CoaguChek® Pro II (Roche, Switzerland), are sensor-based biomarker monitoring systems for targeted diseases such as diabetes, cardiovascular conditions and blood coagulation, respectively (see Table 1).[10–12] These biosensors have capitalised on biological recognition elements such as antibodies or enzymes to function as the molecular recognition element for specific target analyte(s) (*e.g.*, glucose, lactate, cholesterol, and triglyceride) and provide a benchmark for MIP-based biosensors to reach the clinic.[10–12] Furthermore, besides bearing high economic costs, antibodies have sensitive

Table 1 Specifications of commercially available point-of-care biosensors, relating to their advantages and limitations in terms of biosensing capabilities[10–12]

	Prototypes				
Specifications	FreeStyle Libre 2	Accutrend® Plus System			CoaguChek® Pro II
Manufacturer	Abbott, USA	Roche Diagnostics, Switzerland			Roche Diagnostics, Switzerland
Price (£)	58	271			1279
Targeted disease	Diabetes	Cardiovascular			Blood coagulation
Sample material	Interstitial fluid	Capillary blood			Capillary, venous or arterial blood
Analytes	Glucose	Cholesterol	Glucose	Lactate	Triglyceride	Thromboplastin
Sample volume (μL)	—	15–40	15–50	15–50	10–40	≥8
Measuring time (sec)	126–144	180	12	60	Max. 174	9.6–96
Memory capacity	8 h	100 values				2000 results
Operating temperature	10–45 °C	18–35 °C				18–35 °C
Advantages	Data capture in <4 cm range	Determination of 4 different analytes on one platform				Touchscreen
	Suitable for 4–12 years	Test strips have a storage life of up to 18 months[a]				Several built-in quality-control functions (*e.g.*, test strip temperature check and quality control)
	Easily attached to the body	Can store up to 100 different measurements with date and time				Save power mode
	Max. 14 day wear	Great precision and accuracy across the measuring range				Translatable into 13 different languages
	Readings stored every 15 min	Portable hand-held device				WLAN and unique QR code connectivity option
	Rapid data share	Large display – easy to read				
	Excellent accuracy					
	No test strips are necessary					
	Stores up to 90 days of data					
	Portable hand-held device					
	Large display – easy to read					
	Water-resistant					
	Minimally invasive					
	Discreet and convenient					
Limitations	60 min warm-up period	Requires a lancing device				Additional components required
	Finger pricks required (if readings do not match symptoms/expectations)	Additional components required				Requires a lancing device
	Sensor app and website compatibility is selective	Invasive				Invasive
	Daily patterns need at least 5 days of glucose data	Painful				Painful
	Scanning is required every 8 h	Potential blood contamination				Potential blood contamination
	Data transfer is dependent upon mobile connectivity	Expensive				Expensive
	Automatic data upload requires a wireless internet connection or mobile data connection					

[a] From the date of manufacturing.

physicochemical properties, such as, sensitivity to temperature fluctuations and requiring storage conditions below −20 °C.[13] Failure to abide by the storage requirements significantly affects their storage life and, more importantly, the affinity of these molecules with that of the target analyte. The latter is likely to alter their performance as a biosensor, leading to result ambiguity. Therefore, other means of development have considered changing traditional molecular biology practices by obtaining the selectivity of natural antibodies *via* synthetic routes, *e.g.*, soft lithographic processes, systematic evolution of ligands by exponential enrichment, and molecular imprinting.[14]

The field of molecular imprinting historically dates to the 1940s following Pauling's hypothesis that the occurrence of antibodies in human cells is a consequence of the presence of antigens.[15] Pauling attributed the high specificity of the antibody–antigen complex to the behaviour of the antigen, performing as a template, commanding the geometry of the antibody.[15] It is argued that the catalyst of this discovery resulted from Polyakov's development in understanding the importance of solvent selection in 1931, specifically its effect on the pore structure of synthesised silica hydrogels.[16] And since, a variety of synthetic approaches have been generated, giving rise to molecularly imprinted polymers (MIPs) which demonstrate selectivity likened to those of natural antibodies, thereby earning the titles of 'artificial receptors', 'plastic antibodies' and 'antibody mimics', leading to the development of molecularly imprinted technologies (MITs).[17–19]

MIPs have the potential to address many of the current challenges associated with antibody-based diagnostics, including complicated manufacture and handling, long-term stability, and loss of performance in organic media.[17,20–27] MIPs are reasonably inert materials that can be exploited as affordable artificial receptors for biological sensor purposes owed to their selective, specific, biologically stable, and easily tailored (*e.g.*, surface chemistry modifications and/or signalling functionalities) nature in combination with their exceptional physicochemical abilities and extensive shelf-life.[17,20–25,27] Thus, exploitation of these material properties could facilitate improved biomarker detection and analysis compared to clinical biological receptors.[28]

To date, the field of MIPs has been employed in various applications;[28–30] however, this review will evaluate the principles of molecular imprinting for biosensing and evaluate their effectiveness when detecting analytes in biofluids specifically; serum, saliva, cerebrospinal fluid, sweat, urine, nasopharyngeal fluid and tears. Recent progress in integrated MIP sensor technologies for high-affinity analyte detection from complex biofluids will be critically assessed, highlighting state-of-the-art for the progression into disease detection systems in healthcare settings and point-of-need. Throughout this review, the term biosensor will also be applied to sensing devices whereby the recognition element is comprised of a synthetic MIP species. Although this may differ from the International Union of Pure and Applied Chemistry (IUPAC) definition of traditional biosensor terminology, the vast majority of the literature covered in this review considers "biosensors" to include MIP-based sensing devices for the detection of biological analytes.

Mechanisms of molecularly imprinted polymers

MIP synthesis (Fig. 1) is typically achieved *via* the selection of suitable functional monomer(s) that form specific stable

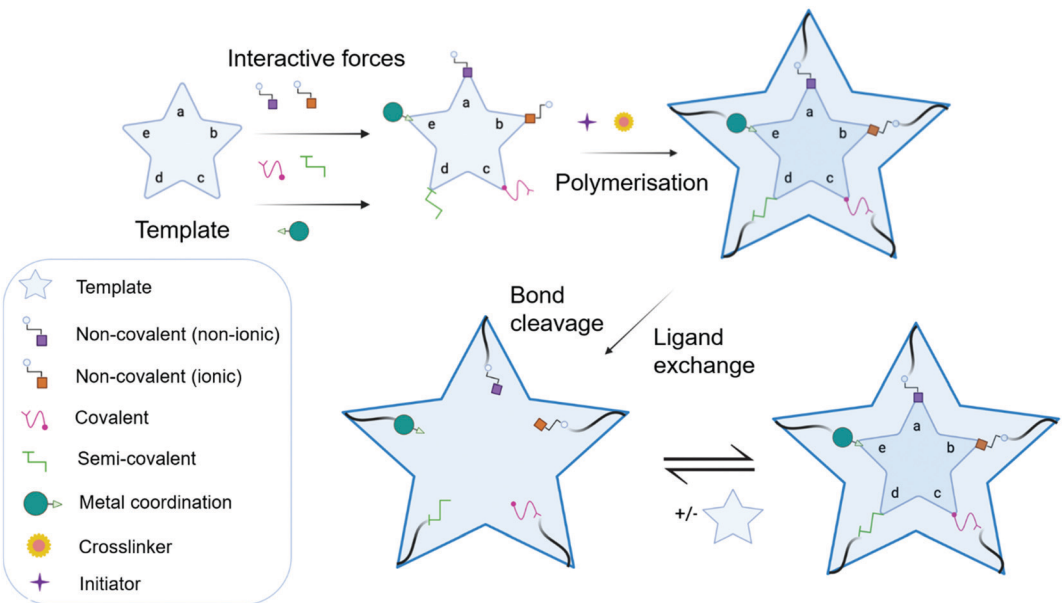

Fig. 1 Molecular imprinting process depicting potential interactions within the template–monomer complex for a MIP synthesised *via* chemical polymerisation, where a, b, c, d, and e, represent non-covalent (non-ionic), non-covalent (ionic), covalent, semi-covalent, and metal coordination, respectively. NB. Interactions depend upon the selected template and monomer(s); therefore, the described interactions are not necessarily all simultaneously at play.

interactions with a template molecule (target analyte).[31,32] The formation of a stable template–monomer complex is critical for the recognition capability of imprinted materials.[33] The spatial arrangement of selected monomers around the template molecule is secured *via* polymerisation, aided by a crosslinking agent (dependent upon the type of molecular interactions selected), forming a three-dimensional polymeric network.[34] Interactions within the polymer matrix, between the newly shaped polymer backbone and template, results in the installation of molecular recognition.[26] These high-affinity binding sites are revealed subsequent to template extraction due to the formation of cavities complementary in shape, size, and chemical functionality to that of the template and closely related functional analogues.[35,36] Molecular imprinting is classified according to the relationship between the MIP and the non-imprinted polymer (NIP) species. NIP synthesis follows the identical protocol employed to produce MIPs while omitting the inclusion of the template molecule. Upon synthesis, NIPs present a three-dimensional network of non-target-specific cavities, where non-specific binding may still occur on the surface thus, acting as a comparative control to selectivity and specificity. In turn, this enables the calculation of quantifiable values for the assessment of both the imprinting factor (*IF*) and the specificity adsorption (α) ratio for sensitivity and specificity determination, respectively.[37] Collectively, these values measure MIP performance, which is largely a consequence of preparative techniques, amongst other factors, including chemical composition (*e.g.*, solvent choice), polymer morphology, template–monomer complexation and their interactive forces.[38–40]

The stability of the template–monomer complex and the energy required for template extraction is governed by the type of intermolecular interactions. For MIPs, molecular interactions are classified as either covalent or non-covalent, contingent on the available functional groups of both template molecules and functional monomer(s) in a suitable solvent.[41] Typically, non-covalent imprinting (Fig. 1a and b) is stipulated by the self-assembly of the template molecule and functional monomer(s) solubilised in a suitable solvent *via* non-covalent interactions (*e.g.*, hydrogen bonding, π–π stacking interactions, or electrostatic forces), followed by the addition of a crosslinking agent to initiate polymerisation.[42,43] Covalent imprinting (Fig. 1c) describes a polymerisable and cleavable template–monomer composite, where the template is covalently bound to the functional monomer(s). In the latter, polymerisation is aided by a crosslinker, after which the template is cleaved off *via* acidic/basic hydrolysis, generating an imprinted species prepared for template rebinding through covalent forces.[44,45] The final approach, semi-covalent imprinting (Fig. 1d and e), exploits both non-covalent and covalent interactions.[25] Like the covalent approach, a template-functional monomer composite is formed, followed by the removal of the template molecule *via* hydrolysis, fabricating cavities for template rebinding through non-covalent bonding interactions.[25]

Commonly, non-covalent interactions are exploited for MIP synthesis, and this is primarily attributed to intermolecular forces, such as hydrogen bonding, encouraging interactions like that of biological recognition systems (*e.g.*, receptor–ligand, enzyme–substrate, and antibody–antigen complexes).[46] Additionally, the ease of template–monomer complex formation, template dissociation and capability to utilise an extensive range of different monomers, has led to non-covalent interactions being widely applied for MIP synthesis.[20] Nevertheless, non-covalent imprinting suffers from limitations in the form of heterogeneous distribution of binding sites and non-specific binding, resultant of excess amounts of functional monomer(s) for pre-polymerisation complex stabilisation.[43] Additionally, there have been reports suggestive of the covalent imprinting approach being superior due to the generation of uniformly accessible imprinted cavities as there is a more homogeneous distribution of binding sites and high selectivity throughout the MIP.[47] However, despite these advantages, covalent imprinting is not widely adopted, attributed to time-consuming template rebinding, limiting its application as a biosensor.[43] Furthermore, covalent imprinting necessitates additional fabrication steps for template–monomer composite stabilisation *via* covalent bond formation. In particular, covalent forces are restricted to diols, ketones, aldehydes, carboxylic acids, and amines.[45] Semi-covalent interactions, like covalent interactions, can produce polymers with high selectivity; however, polymers formed *via* these interactions can suffer from non-specific binding due to uncleaved template molecules, occupying binding sites.[37]

The success of these antibody mimics has progressed their application for the employment of sensory components, detecting bioanalytes (*e.g.*, electrolytes, metabolites, amino acids, proteins, and hormones) located within bodily fluids.[48–50] These bioanalyte-rich media, including but not limited to, saliva, tears, and sweat offer essential information regarding patient health.[51] By considering alternative biofluids, other than the current gold standard – arterial blood – enables biomarkers to be readily accessed in a minimally invasive manner, laying the foundations for their evolution from bench to bedside.[28–30,52]

Methodologies to produce molecularly imprinted polymers with example bio-applications

Today, molecular imprinting is broadly employed for various applications, such as biosensing, chromatographic separation and solid-phase extraction, among others.[52–55] Traditionally, MIPs are formed *via* free-radical reactions employing preparation methods such as bulk, precipitation, emulsion, and suspension techniques (Fig. 2a–d).[56] The degree of imprinting within a polymeric network is defined as the *IF* efficiency and can be calculated as shown by eqn (1), where the equilibrium binding capacity (Q), *i.e.*, the amount of analyte bound by MIP and NIP species, denoted by Q_{MIP} and Q_{NIP}, respectively, is first determined. Q (eqn (2)) describes the divergence between the initial amount of target analyte in the introduced solution mixture relative to the amount in the supernatant, where C_i, C_f, m and V define the initial concentration of the target analyte in the introduced mixture, the equilibrium concentration of the target analyte in the solution mixture, the mass of the polymer and volume of the analyte solution

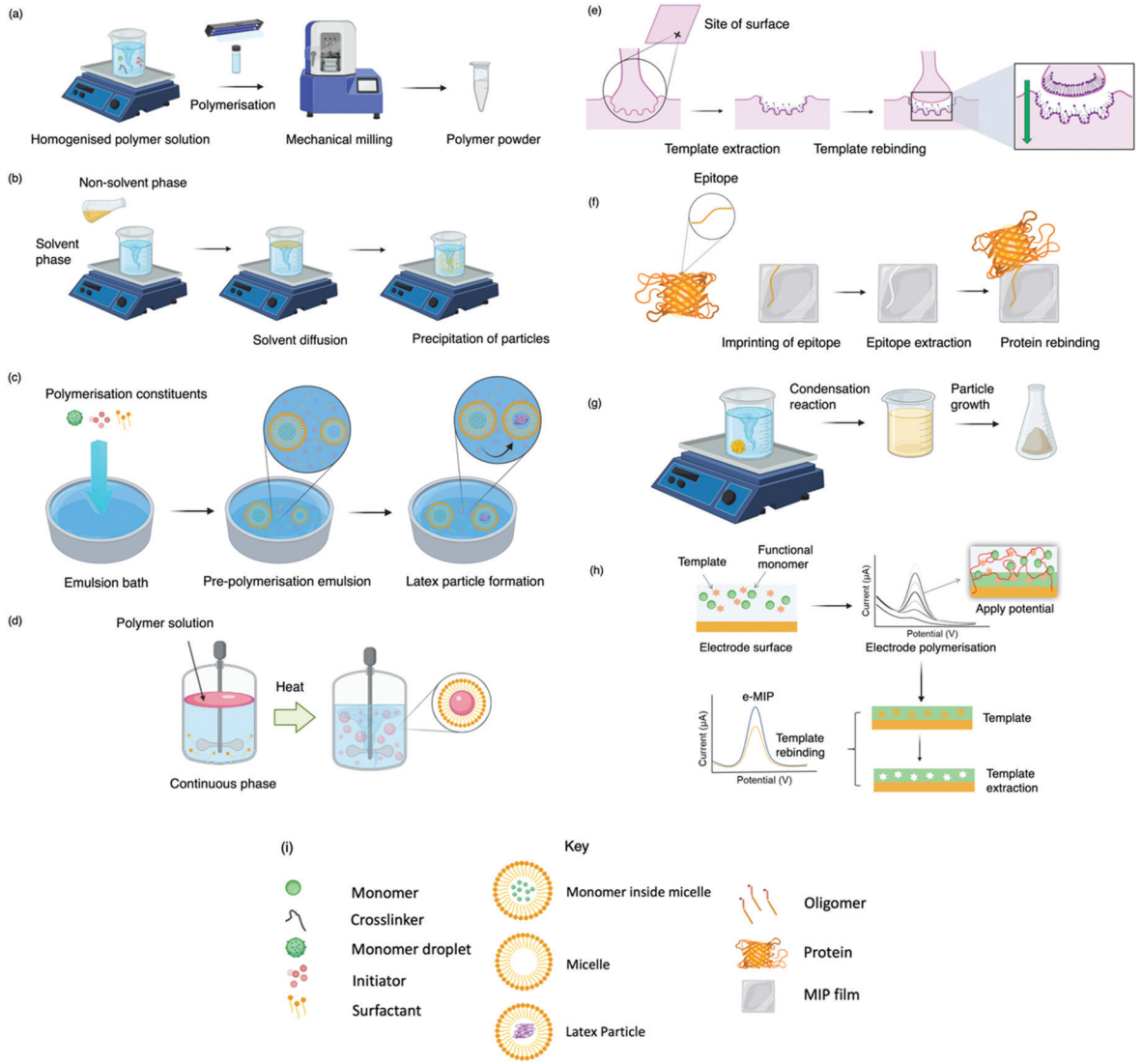

Fig. 2 Illustrative diagram depicting a range of different polymerisation techniques including: (a) bulk, (b) precipitation, (c) emulsion, (d) suspension, (e) surface, (f) epitope, (g) sol–gel, (h) electropolymerisation, and (i) each technique's associated key.

mixture, respectively.[37,57–59] Additionally, Q, can also be used to determine the specificity adsorption ratio (a), which describes the degree of selectivity of MIP species in relation to the NIP species, as shown by eqn (3).[57] *IF* and α values exceeding 1 are indicative of a good degree of molecular imprinting and target analyte specificity, respectively.

$$IF = \frac{Q_{\mathrm{MIP}}}{Q_{\mathrm{NIP}}} \quad (1)$$

$$Q(\mathrm{mol/g}) = \frac{(c_{\mathrm{i}} - c_{\mathrm{f}})}{m} V \quad (2)$$

$$\alpha = \left(\frac{Q_{\mathrm{MIP}} - Q_{\mathrm{NIP}}}{Q_{\mathrm{MIP}}}\right) \quad (3)$$

Bulk polymerisation (Fig. 2a) proceeds with the initiation of a soluble radical initiator in the presence of soluble monomer(s) (functional monomer and crosslinker) upon thermal or ultraviolet radiation exposure.[60,61] Precipitation polymerisation (Fig. 2b) describes a homogeneous polymer solution consisting of soluble monomer(s) and initiator in a continuous phase.[60,61] Upon initiation, a heterogeneous mixture is formed in which the insoluble polymer precipitates out.[62] Olcer *et al.* utilised bulk and precipitation polymerisation to prepare a highly selective and reusable (up to five times) MIP to detect endocrine-disrupting chemicals, specifically, ibuprofen in drinking and tap water samples.[60] In the study, ibuprofen, methacrylic acid, trimethylolpropane trimethacrylate were employed as template molecule, functional monomer, and crosslinker in a 1 : 8 : 20 molar ratio, respectively, with 4,4-azobis(4-cyanovaleric acid) and acetonitrile as initiator and porogen. Precipitation polymerisation was more successful in formulating a MIP with higher template affinity compared to the bulk-synthesised MIP.[60] The imprinted polymer prepared *via* precipitated means showed an approximately two-fold increase in sorption capacity compared to its control (non-imprinted

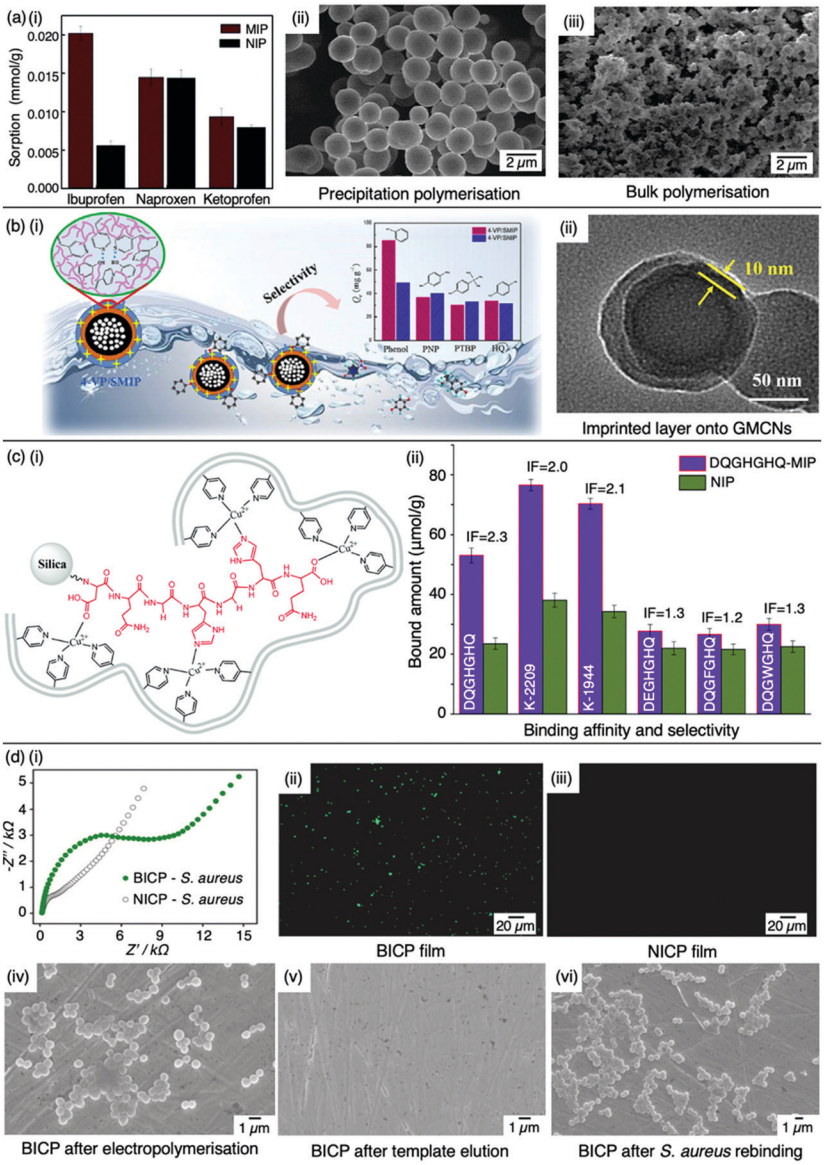

Fig. 3 Molecular imprinting through different synthesis routes. (a) Comparison of precipitation vs bulk polymerised MIPs. (i) Sensitivity and selectivity of ibuprofen MIPs prepared *via* means of precipitation in the presence of structurally related compounds; (ii) scanning electron microscopy (SEM) image of MIP prepared *via* precipitation polymerisation, and; (iii) SEM image of MIP prepared *via* bulk polymerisation. Reproduced with permission from ref. 60, Copyright 2017 Royal Society of Chemistry. (b) Bulk polymerised MIPs presenting glucose-derived microporous carbon nanospheres. (i) Schematic illustration of phenol extraction from wastewater using a highly selective surface imprinted MIP; (ii) transmission electron microscopy image of 4-vinyl pyridine surface imprinted MIP. Reproduced with permission from ref. 87, Copyright 2020 Elsevier. (c) Epitope imprinted silica-conjugated MIP peptides. (i) Polymeric mixture of epitope-containing peptides secured *via* polymerisation; (ii) competitive binding of epitope-MIP with structurally similar peptide interferants. Reproduced with permission from ref. 88, Copyright 2016 Royal Society of Chemistry. (d) Bacteria-imprinted conducting polymer film. (i) Comparative electrochemical response of bacteria imprinted conductive polymer (BICP) sensor and corresponding non-imprinted conductive polymer (NICP) as control; (ii and iii) fluorescence images of BICP and corresponding NICP films after *staphylococcus aureus* retention; (iv–vi) scanning electron microscopy images of varying polymer films modified gold electrodes. Reproduced with permission from ref. 89, Copyright 2021 Elsevier.

polymer, NIP), calculated at 0.0387 mmol g^{-1} and 0.0235 mmol g^{-1}, respectively at 50 mg L^{-1}. Selectivity was demonstrated in the presence of compounds sharing structural likeness to that of ibuprofen, namely naproxen and ketoprofen (Fig. 3(a-i)). The success of the precipitation technique over the bulk technique was attributed to the MIP's spherical nature (Fig. 3(a-ii)), providing greater surface area compared to the monolithic MIP (Fig. (3(a-iii))), thus allowing for more selective cavity sites at the surface of the polymer, arguably the principal contribution to sorption performance.[60]

Despite bulk polymerisation being considered a simplistic approach, some synthesis protocols can require mechanical milling and, if necessary molecular sieving to provide uniform particle shapes and sizes.[63,64] However, milling could reduce MIP capturing capacities by damaging or distorting imprinted interaction sites.[65] Regardless of the limited control over the

physical form of the obtained imprinted species, many MIP publications still employ the bulk polymerisation approach, possibly due to reproducibility and simplicity with respect to the preparation and formulation of this polymerisation process.[60,61,63,66] Bulk polymerisation limitations have led to the development of alternative approaches, including *in situ* prepared monoliths, molecularly imprinted monoliths, MIP membranes, and MIP beads.[22,67–71] Precipitation polymerisation (Fig. 2b) is credited to the processes improved heat control and direct preparation of large-scale production.[72] However, precipitation polymerisation requires a greater volume of porogen and more rigorous reaction control compared to bulk polymerisation.[72–74]

Emulsion polymerisation (Fig. 2c) describes the dispersion of monomer(s) and surfactant(s) in an emulsion of either water-in-oil or oil-in-water. Polymer spheres are formed *via* the generation of free radicals by an initiator (water- or oil-soluble – dependent upon polymerisation type).[75] In a recent study, Zhao *et al.* established a MIP to purify solanesol, an essential pharmaceutical intermediate and an organic substance to produce anti-ulcer and anti-cancer drugs *via* emulsion polymerisation. In this study, the effects of varying quantities of MIP chemical composition were investigated for MIP functionality performance purposes. Zhao *et al.* successfully synthesised spherical solanesol MIP (SS-MIP) microspheres, with particle sizes ranging between 50–500 mm, using solanesol, methyl methacrylate, ethylene glycol dimethacrylate and potassium persulfate, performing as template species, functional monomer, and crosslinker, in a 1 : 8 : 30 molar ratio, respectively. SS-MIP performance was demonstrated by maximum absorption retention (Q_{max}) of 56.97 mmol g^{-1} and reported an *IF* of 2.51.[76] Although the fabricated SS-MIP showed good adsorption properties, more research is required to validate the performance of this means of polymerisation, including, but not limited to: (a) improved protocols for the formation of uniformly shaped and sized SS-MIPs, (b) investigation into the recognition sensitivity and specificity of SS-MIPs, and (c) study of SS-MIP applications.[76] Ma *et al.*, however, successfully demonstrated a large-scale applicatory function of SS-MIPs for high-purity solanesol extraction from tobacco leaves using chromatographic methods *via* suspension polymerisation, where methacrylic acid, ethylene glycol dimethacrylate, and 2,2′-azobisisoheptonitrile were used as functional monomer, crosslinker and initiator, respectively. The synthesised spherical SS-MIPs (particle diameter 250–350 mm) exhibited a Q_{max} of 107.3 mmol g^{-1} and *IF* of 3.9.[77]

In suspension polymerisation (Fig. 2d), a dispersed heterogeneous mixture of droplets is formed that undergoes polymerisation, ultimately forming polymer spheres.[78] Gomes *et al.* produced polyphenol MIPs *via* precipitation and suspension polymerisation to determine the most superior process for morphology and performance, using polydatin, a precursor of resveratrol available in vegetable extracts, as a template.[69] Polydatin is an important detectable target due to its antioxidant and anti-inflammatory capabilities, rendering it a valuable chemical for disease treatment.[79] Gomes *et al.* synthesised a range of MIPs for the amphiphilic polydatin template through a parametric study that assessed a variety of functional monomers, crosslinkers, and solvents for the assessment of non-covalent interactions (including hydrophobic/hydrophilic interactions) between the template–monomer complex and their effects on imprinting efficiency. For natural extracts, hydrophilic/hydrophobic interactions are inevitable; thus, the adjustment of solvent polarity is critical for the isolation of different polyphenols.[69] In this study, polydatin, 4-vinylpyridine, 2,2-azobisisobutyronitrile, water/methanol, and sorbitan mono-oleate (Span 80) as template species, functional monomer, initiator, solvent, and surfactant, respectively, presented a Q_{max} of ~300 mmol g^{-1}, greater than literature reported values.[80–84]

Some of the previously discussed polymerisation techniques can suffer from poor imprinted cavity access due to embedded binding sites, incomplete template removal and slow mass transfer rates. Surface imprinting (Fig. 2e), on the other hand, generates materials with large surface areas (surface-to-volume ratio) and high porosity owed to their distribution of externally available binding sites. Arranging cavity sites in this way is favourable for removing and rebinding the target analyte as imprinted cavities are readily exposed.[85,86] Moreover, these surfaces are controllable, show low migration resistance towards selective adsorption, bypassing the template embedding phenomenon, resulting in greater adsorption capacities.[69]

Recent studies have shown surface or outer layer modifications of MIPs to be a popular method of molecular imprinting, utilising specific carriers such as silica, polystyrene microspheres, quantum dots, metal–organic frameworks, magnetic nanoparticles, and carbon nanomaterials.[87,90–93] Qu *et al.* recently used surface molecular imprinting to fabricate a highly selective MIP prepared on glucose-derived microporous carbon nanospheres for the removal of phenol (Fig. 3(b-i)), a highly toxic substance found in wastewater which can affect the cardiovascular and central nervous system.[94,95] Glucose-derived microporous carbon nanospheres were employed as support materials due to their rich pore structures and surface located oxygenic functional groups, where active layers were stabilised *via* silane coupling agents. An optimal polymeric mixture was synthesised using phenol, 4-vinylpyridine, ethylene glycol dimethacrylate, 2-methylpropionitrile, and toluene as template molecule, functional monomer, crosslinker, initiator, and solvent system in a 1 : 3 : 1.8 : 0.07 ratio, respectively. The assembly of this surface imprinted crosslinked polymer (Fig. 3(b-ii)) displayed a Q_{max} of 85.72 mg g^{-1}. The successful isolation of phenol from wastewater was displayed by the relative selectivity factors (a) of phenol *versus* three interfering molecules; hydroquinone, *p*-nitrophenol and *p-tert*-butylphenol, valued at 8.38, 7.96 and 6.67, respectively, highlighting the selective capabilities of this synthesised MIP.[94]

Surface imprinting technology was also employed by Liu *et al.* to develop highly sensitive and specific magnetic MIPs (MMIPs). MMIPs with an average particle size of 2 μm were prepared *via* graphite-like carbon nitride–iron oxide nanoparticles as support matrices for the adsorption of atrazine, a herbicide with known carcinogenic effects. Adsorption isotherms

demonstrated that MMIPs (1.82 mmol g^{-1}) formulated by atrazine, methacrylic acid, ethylene glycol dimethacrylate, 2,2-azobisisobutyronitrile, and chloroform as template molecule, functional monomer, crosslinker, initiator, and solvent system, respectively, showed a greater adsorption capacity compared to its control counterpart (MNIP, 0.875 mmol g^{-1}) at 80 mmol L^{-1}. Additionally, adsorption of atrazine molecules was greater when compared to structural analogues (ametryn, atratin, hexazinoneas), demonstrating high selectivity towards atrazine pesticides for the detection of atrazine from complex substances.[96]

Epitope imprinting (Fig. 2f) exploits short characteristic regions of biomolecules (*e.g.*, peptides) performing as templates.[97] Epitope MIPs (EMIPs) can overcome concerns surrounding the imprinting of bulky macromolecular structures, often burdened with diffusion issues within the highly crosslinked three-dimensional polymeric network and conformational changes due to harsh polymerisation conditions and environments.[97,98] EMIPs encourage the use of conventional monomers, facilitating improved template extraction procedures, and are more cost-effective as they avoid the need for an entire biomolecule, making it a valuable technique for the application of protein studies.[99,100] Like traditional imprinting methods, the epitope approach can be utilised *via* bulk or surface imprinting, depending upon the desired template–monomer complex interactions.[101] Template immobilisation onto a supporting matrix is critical for successful EMIP formation, where studies have reported the preparation of templates *via* boronate affinity, physical adsorption, metal ion chelation, and covalent bonding.[98,102,103]

Xing *et al.* developed a novel controllable oriented surface imprinting approach, utilising boronate affinity-anchored epitopes to imprint protein templates.[98] This study was centred around the 2-microglobulin (b_2M) protein sequence, where abnormal concentration levels are associated with diseases such as multiple myeloma.[104] The C-terminus nonapeptide, attached with a lysine, was selected as the template epitope, with 2,4-difluoro-3-formyl-phenylboronic acid acting as the coordinating ligand. Consequential of boronate affinity, the glycated epitope was immobilised onto boronic acid-functionalised magnetic nanoparticles, coated with multiple silylating agents, facilitating template–monomer interactions *via* polycondensation reactions in a monomer ratio of 10 : 10 : 20 : 60, respectively.[98] The synthesised glycated epitope-imprinted magnetic nanoparticles (average diameter 150 nm) presented an imprinting efficiency percentage and *IF* value of 54.2% and 5.8, respectively. The study further demonstrated the successful removal of b_2M-epitope and protein using the synthesised glycated b_2M EMIP, through fast equilibrium kinetics (~20 min), attributed to easily accessible surface imprinted cavities. Additionally, b_2M protein showed greater selectivity, attributed to the highest *IF* calculated at 6.5, compared to competitive analogous proteins ribonuclease A, ribonuclease B, horseradish peroxidase, and bovine serum albumin. Moreover, the imprinted species demonstrated long-term storage capabilities (*ca.* three months) with a minimal reduction in sensitivity performance (13.4% decrease) and withstood a total of six consecutive activities of rebinding.[99]

Tang *et al.* opted for the covalent approach to prepare two biomarker peptides (K-2209 and K-1944), reflective of gastric and liver cancer diagnosis, using heptapeptide (DQGHGHQ) as the epitope template.[102] Porous silica was retained as a sacrificial substrate for template molecule immobilisation.[105] Spherical imprinted particles were synthesised *via* hierarchical imprinting polymerisation, utilising the metal coordination interaction between copper(II) oxide, the template species, and 4-vinyl pyridine (performing as both functional monomer and coordinating ligand) for the formation of binding sites (Fig. 3(c-i)).[88] The optimal pre-polymerisation mixture was formed of template, aqueous copper acetate, 4-vinyl pyridine, ethylene glycol dimethacrylate (crosslinker), and 2,2-azobisisobutyronitrile (initiator) in a 1 : 6 : 12 : 30 molar ratio, respectively, dissolved in acetonitrile. DQGHGHQ-MIP exhibited a 71–88% recovery performance for the K-1944 and K-2209. This study demonstrated the potential of epitope imprinting to aid biomarker screening for cancer diagnosis through individual and competitive batch binding experiments. The individual experiments highlighted the highest *IF* (2.2) for the DQGHGHQ-MIP, followed by K-2209 (2.0) and K-1944 (2.0), and competitive binding results exhibited a *ca.* 1.7-fold selectivity towards the DQGHGHQ-MIP apropos to its competitive peptide counterparts (DQGWGHQ, DQGFGHQ and DEGHGHQ) (Fig. 3(c-ii)).[102]

The sol–gel technique (Fig. 2g) offers high solvent and thermal stability, material homogeneity at the molecular level, and a one-pot fabrication process.[58] Commonly, sol–gel imprinting utilises tetra-methyl or -ethyl orthosilicate as a precursor to introduce the template species into the polymeric framework.[58] The polymeric mixture undergoes hydrolysis followed by polycondensation reactions, generating crosslinked polymeric gels.[106] Sol–gel imprinting has attractive characteristics, including simple preparative techniques, controllable porosity and surface area, and easily tailored chemical functionality for enhanced selectivity.[58] Unlike radical polymerisation, where polymer network formation has a dependency on both temperature and the choice of organic solvent (*e.g.*, chloroform), this technique can be performed at room temperature with environmentally friendly solvents (*e.g.*, water).[107] For instance, Guoning *et al.* used Tween® 20, a non-ionic water-soluble surfactant, to encourage mild hydrolysis to develop a surfactant-mediated sol–gel system to fabricate protein MIP layers, utilising 3-(methacryloxy)propyltrimethoxysilane as crosslinker.[108] Human serum albumin, one of the most abundant proteins present in blood plasma, was selected as the target protein as this biological analyte can correspond to ailments such as kidney disease.[109,110] The authors formed a homogenous protein–polymer mixture, with no protein deformation within the organic solvent system (methanol and toluene) being reported. MIP layers were stabilised onto iron(II, III) oxide nanospheres to encourage rapid magnetic separation and immobilisation. Finally, ovalbumin was employed as a protein blocking agent to improve MIP selectivity by reducing the effects of non-specific binding. This method of molecular imprinting demonstrated a limit of detection (LoD) of 0.3 μg mL^{-1} and recovery ranges of 85.4–104.5%, where the authors stated the significance of the

selective species with the potential to replace their biological counterparts (*e.g.*, antibodies).[108] Considering healthy human serum albumin levels found in urine samples are ~ 30 mg mL^{-1}, the authors have proposed a very sensitive means to detect the onset of kidney disease.[111]

Finally, MIPs can be produced *via* electropolymerisation (Fig. 2h). Established in the late '90s, electropolymerisation rapidly emerged as a strategy to develop thin MIP films *via in situ* spatial confinement of polymer layers directly onto the surface of an electrode.[112,113] This form of polymerisation is initiated by the oxidation (voltage- or current-induced) of a specific monomer in an electrochemical cell, facilitating polymer growth.[114] Electropolymerisation enables precise control over film thickness and shows good compatibility with aqueous media.[115]

Malitesta *et al.* prepared and characterised the first electrosynthesised MIP using glucose and *o*-phenylenediamine as template molecule and functional monomer, respectively.[116] This pioneering study utilised *o*-phenylenediamine, a known enzyme-entrapping membrane previously employed to fabricate biosensors, to confirm the feasibility of an electropolymerised MIP *via* the exploitation of a neutral template.[117] Direct analytical communication between the transducer element, quartz crystal microbalance and synthetic MIP species was established.[116] These promising findings encouraged Özcan *et al.* to fabricate an electropolymerised MIP *via* a modified pencil graphite electrode to detect paracetamol (a regularly used analgesic and antipyretic drug) in clinical and pharmaceutical samples.[118,119] Polypyrrole (pyrrole, monomer) films were processed *via* cyclic voltammetry deposition in the presence of lithium perchlorate (supporting electrolyte) with (MIP synthesis) or without (NIP synthesis) paracetamol.[119] Differential pulse voltammetry was used to evaluate MIP and NIP performance, with a LoD of 7.9×10^{-7} M (3σ), highlighting the imprinted species sensitivity towards paracetamol. Moreover, this MIP demonstrated a constant and reproducible response (1.3%, relative standard deviation (RSD) ($n = 6$)), even when in the presence of competitive species (*e.g.*, dopamine, phenacetin, ascorbic acid, phenol and D-glucose), highlighting the MIP sensor's selectivity towards paracetamol.[119]

More recently, Wang *et al.* designed a MIP electrochemical sensor using the conductive monomer 3-thiophenacetic acid for rapid sensitive, and label-free detection of *Staphylococcus aureus* (*S. aureus*), a Gram-positive pathogen responsible for a wide range of clinical infections.[89,120] The conductive MIP film was deposited on the surface of a gold electrode, negating the use of toxic organic solvents or a crosslinking agent. Optimised conditions exhibited a significantly low LoD and very fast kinetic recognition valued at 2 CFU mL^{-1} and 10 min, respectively. This impedimetric sensor verified good MIP sensitivity and selectivity with respect to electrical impedance spectroscopy responses compared to NIP species (Fig. 3(d-i)) and structural analogues, including Gram-positive *Listeria monocytogenes* and Gram-negative *Escherichia coli* (*E. coli*) O157 and *Salmonella Paratyphi* B. Additionally, fluorescence imaging was utilised to assess the presence of *S. aureus* on the surface of the bacteria-imprinted conductive polymer film, reinforcing successfully installed *S. aureus*-specific recognition cavities, where target bacteria was visibly detectable on the MIP species (Fig. 3(d-ii)) and evidently absent on the NIP species (Fig. 3(d-iii)). Moreover, SEM images captured different polymer film-modified electrodes during the process of bacterial imprinting and recognition, verifying that *S. aureus* had successfully been embedded on the poly-3-thiophenacetic acid matrices (Fig. 3(d-iv–vi)). Ultimately, Wang *et al.*'s chosen polymerisation techniques have paved the way for potential bacteria-imprinted conductive polymer films for pathogen detection in applications such as food and water safety. The discussed polymerisation methods are summarised in Table 2.[89]

Following polymerisation completion, the template requires removal from the three-dimensional polymer network to finalise the molecular imprinting process. Template removal is often achieved *via* washing methods using various solvents from aqueous-based to alcohols, and less commonly, by exposing the final product to elevated temperatures or electrochemically.[121–123] Optimal template removal conditions should follow a simplistic approach, operating within a reasonable timeframe and using a minimal amount of environmentally friendly solvent(s).[124] It is important to note that the NIP usually does not undergo the template removal step, as would be expected. However, for complete comparative analysis, both the MIP and NIP should be exposed to consistent chemical conditions throughout their syntheses. In addition, evidence has suggested that skipping the template extraction protocol for the NIP has led to unrealistic and overstated selectivity factors to that of the MIP.[125]

Development of MIPs as biosensors for point-of-care diagnostics

Molecular imprinting techniques have seen an expansion in target species, including cells and microorganisms.[129–131] For example, the selective identification of microorganisms (*e.g.*, pathogenic bacterial strains) in biological media *via* artificial MIP biosensing systems has gained widespread attention as a new class of sensing materials that permits for processing-free whole-cell bacterial detection.[129] Traditionally, bacterial detection relies on cultures and antibiotic susceptibility tests, immunological assays, genome sequencing, and biochemical testing, often associated with laborious, expensive, and time-consuming practices.[132,133] Recent work has described how utilising MIPs can provide a unique approach for the identification of bacterial pathogens.[134–139]

Shen *et al.* integrated MIT to fabricate bacteria imprinted polymer (BIP) beads for microbiological disease detection *via* Pickering emulsion polymerisation.[140] BIP beads were synthesised in phosphate-buffered saline and prepared for two different groups of bacteria, rod-shaped *E. coli* (*E*-BIP) and spherical-shaped *Micrococcus luteus* (*M. luteus*) (*M*-BIP), to determine whether whole-cell recognition performance of imprinted receptors was affected by cell shape. Prior to template extraction, polymer bead surfaces indicated the presence of *E. coli* (Fig. 4(a and b)); however, post-template extraction, only custom-made imprinted

Table 2 Summary of the strengths and drawbacks of different molecularly imprinting polymer technology preparation methods

MIP Preparation Techniques		Strengths	Drawbacks	Ref.
Radical	Bulk	– Fast preparation methods without the use of sophisticated equipment – Synthesis of large batches – Affordable synthesis – Polymer mixture is prepared in liquid form – Additional solvent is not required – MIP particle sizes can be readily adjusted	– MIPs require mechanical grinding and sieving - could destroy installed cavities – Large volumes of porogen are obligatory	56, 60 and 126
	Emulsion	– Addition of surfactant(s) or stabiliser(s) unrequired – Forms high yield of monodispersed particles – Polymers are suitable for aqueous environments	– Emulsifying agent, hydrophobic monomer(s), and hydrophilic initiator is mandatory	56, 76 and 126
	Suspension	– Simple synthesis – Forms uniform MIP microspheres – Forms highly porous MIP films	– Polymeric mixtures involve both aqueous and organic phases, but many monomers are not water-soluble – Large range between produced particle sizes (up to several hundreds of micrometres) – Initiator and monomer must be hydrophobic – Requires surfactant(s) and stabiliser(s)	56, 69 and 126
	Precipitation	– Quick and simple – High yields of uniformly shaped MIP beads – Individual polymeric chains are cultivated into microspheres – Polymeric mixtures do not require porogens	– Only successful if polymeric chains are of the appropriate size to reach insolubility within the polymeric reaction mixture – Requires large quantities of template	56, 61 and 126
Sol–gel		– Reaction solvent(s) are environmentally friendly – Pore sizes can be readily controlled – MIPs have excellent thermal and mechanical stability	– MIPs have low sensitivity – Polymerisation suffers from slow kinetics – Solvent polarity, mechanical stirring, and polymerisation temperature affect the size of the particles	56, 58 and 126
Epitope Imprinting		– Templates are small - can easily be removed – Reduction in structural complications improves specificity and selectivity – Synthesised with organic solvents – Affordable	– Suitable protein regions must be screened – Surface charges need consideration	56, 97 and 126
Surface Imprinting		– Less template required – Easier template extraction – Installed cavities are more accessible to template molecules providing favourable binding kinetics	– Fewer cavities are formulated - decreased sensitivity	56, 126 and 127
Electropolymerisation		– Direct polymerisation onto the electrode surface	– Recognition performance is governed by film thickness, choice of monomer(s), electrode potential, among others – Choice of monomer(s) are limited	56, 115, 126 and 128

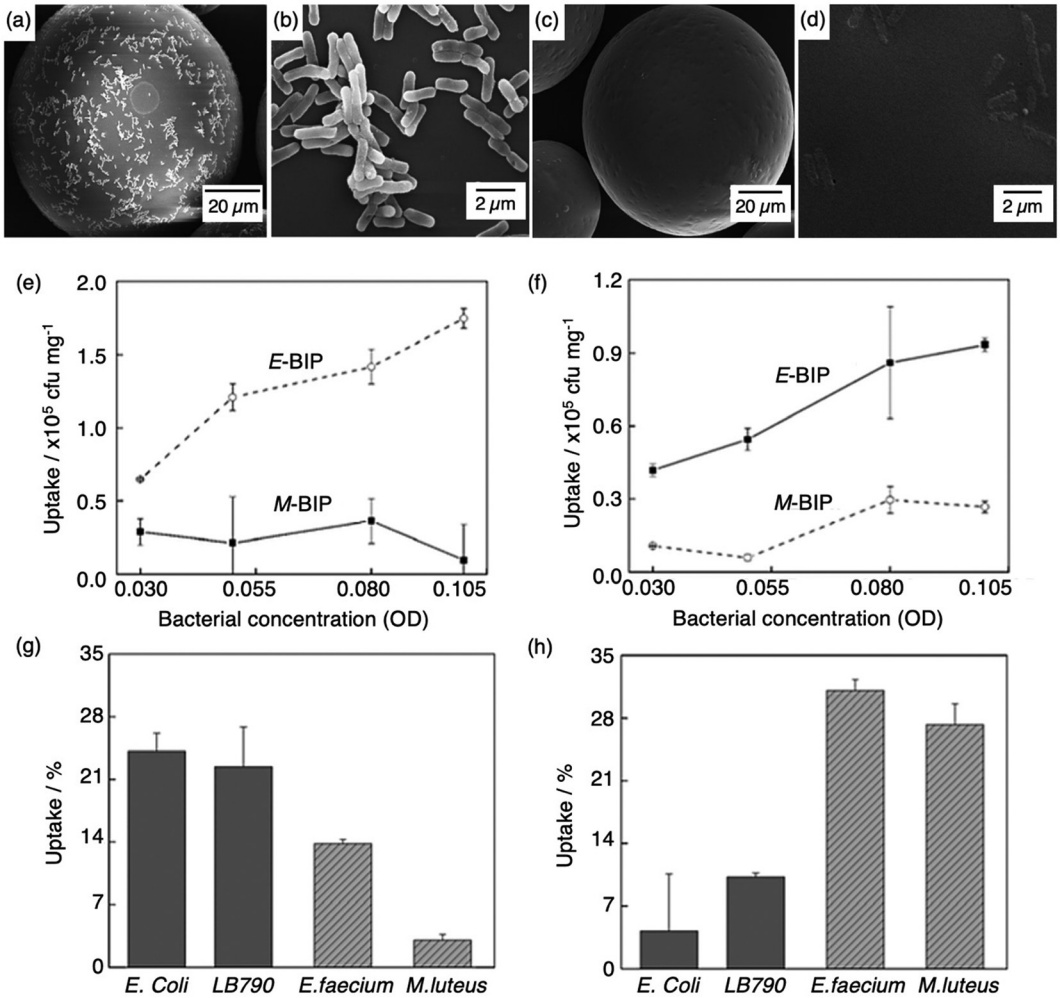

Fig. 4 Bacterial imprinting at Pickering emulsion interfaces. (a and b) SEM images of *E. coli* imprinted polymer beads before template extraction and (c and d) after template extraction; (e and f) sensitivity and selectivity of *E*-BIP and *M*-BIP demonstrated by *E. coli* and *M. luteus* uptake, and (g and h) uptake of different cells. Reproduced with permission from ref. 140, Copyright 2014 John Wiley & Sons. † *Escherichia coli* (*E. coli*), *Lactobacillus sakei* (LB790), *Enterococcus faecium* (*E. faecium*), *Micrococcus luteus* (*M. luteus*).

cavities were visibly present on the surface (Fig. 4(c and d)). Both *E*-BIP and *M*-BIP beads demonstrated favourable binding of the analogous template cells, indicative of preferential BIP bead selectivity between rod- and spherical-shaped bacteria cells (Fig. 4(e–h)).[140] Thus, this study highlighted a practical way to fabricate bacterial recognition sites *via* molecular imprinting, developing possibilities towards biosensors for real-time examination of whole-cell bacteria species in biofluids.

Roushani *et al.* introduced a new diagnostic method for the detection of *Acinetobacter baumannii* (*A. baumannii*), one of the most challenging agents of nosocomial infections worldwide.[141] MIP synthesis was achieved *via* electropolymerisation of the template (*A. baumannii*) and the functional monomer (dopamine) on the surface of a glassy carbon electrode. Electrochemical properties were used to characterise the performance of the MIP and analogous NIP modified electrode, including cyclic voltammetry and impedance spectroscopy, in a hexacyanoferrate (operating as the electrochemical probe) redox system. This sensor presented a linear range of 10^2–10^7 CFU L^{-1} with a 30 CFU L^{-1} LoD in human blood serum samples, the first of its kind.[141]

MIPs have also been integrated with quartz crystal microbalances for facile, cost-effective, high-resolution, and label-free mass sensing, owing to this device's ability to measure very small mass changes on a quartz crystal resonator in real-time. This type of sensor has been extensively utilised for analytical purposes, attributed to the technique's high sensitivity and on-line acquisition aptitude.[142,143] Quartz crystal microbalances are generally composed of a quartz disc incorporated with electrodes, and in terms of MIP sensors, they function by measuring the disturbances in frequency resonance resultant of target analyte adsorption/binding based on the Sauerbrey equation.[144] Therefore, changes in resonance energy are proportional to interactions between the target analyte and imprinted cavity recognition sites.[145]

Tokoname *et al.* used a quartz crystal microbalance to recognise the rod-shaped bacilliform bacteria, where sensor performance was improved by integrating MIP technology with dielectrophoresis. The target bacterial species was precisely

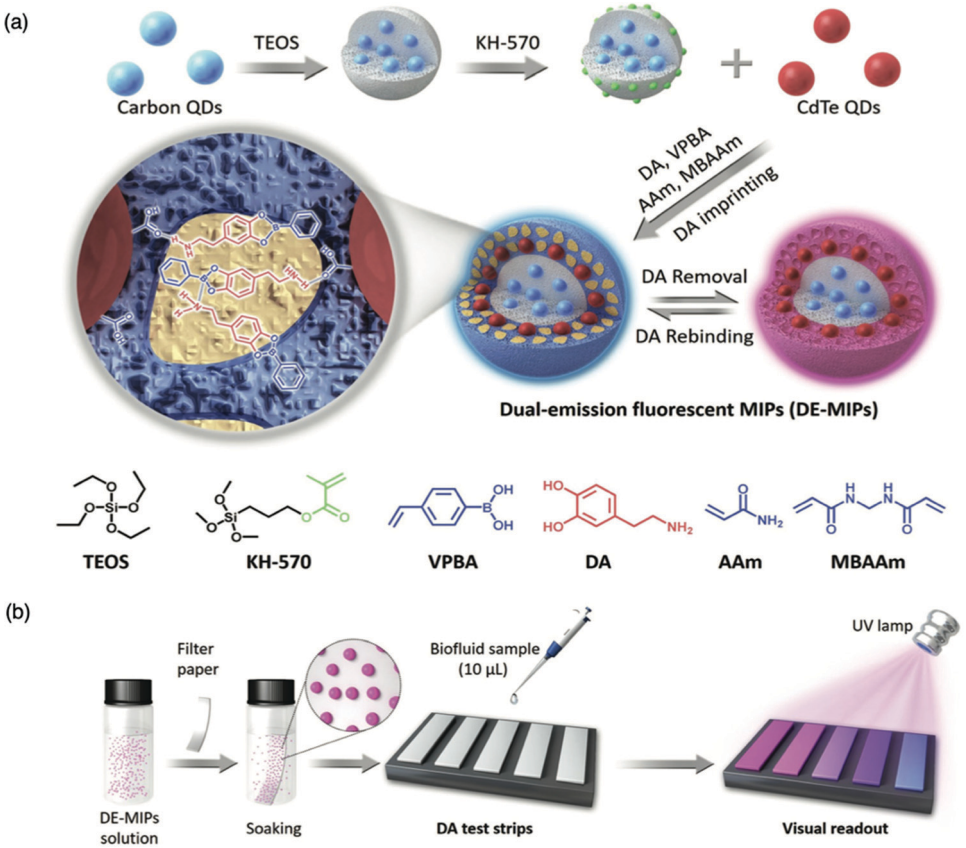

Fig. 5 Molecularly imprinted fluorescent test strip for dopamine detection in biofluids. (a) Production of dual-emission fluorescent molecularly imprinted polymer nanoparticles (DE-MIPs) with specific dopamine recognition, and (b) DE-MIPs-coated filter paper as an easy dopamine test strip optical detection. Reproduced with permission from ref. 147, Copyright 2019 John Wiley & Sons.

printed on the surface of a polypyrrole film, and the corresponding imprinted cavities were created by extracting the target template upon overoxidation. The integration of both technologies allowed real-time and selective detection of bacilli from apple juice samples with a LoD as low as 10^3 CFU mL^{-1} within 180 s, exclusive of any pre-treatment. These cavities showed high selectivity and were capable of successfully differentiating competitive rod-shaped bacterial species, including *Acinetobacter calcoaceticus*, *E. coli*, and *Serratia marcescens*, highlighting a simple and rapid bacterial detection method for potential future clinical point-of-care testing.[146]

For the detection of smaller biomolecules, Wang *et al.* integrated dual-emission fluorescent MIPs (DE-MIPs) into a facile test strip for the visual detection of dopamine *via* colorimetric analysis.[147] Dopamine sensing is vital for the diagnosis, prevention, and management of neurological disorders including, but not limited to, Parkinson's disease, schizophrenia, and Huntington's disease.[148–150] Dopamine selective DE-MIPs were prepared *via* the combination of two types of quantum dots with red and blue colour emissions using imprinting technology.[56,151] The blue quantum dots were implanted into silica nanocores, preserving continuous fluorescent intensity, whilst the red quantum dots were hybridised into the imprinted polymer shell, encouraging dopamine interaction and stimulating fluorescence quenching during dopamine rebinding (Fig. 5a). DE-MIPs were layered onto a filter paper, formulating a dopamine test strip (Fig. 5b). Serum samples of 10 mL demonstrated dopamine detection within 180 s with a low LoD of 100–150 nM, showing sensitive detection to physiological dopamine levels. Thus the authors successfully prepared a facile and efficient strategy for rapid, visual, and on-site detection of physiologically important species available in biofluids.[147]

In addition, surface plasmon resonance, a non-invasive and label-free detection, is another technique that can be employed to develop MIPs into point-of-care biosensors.[153] Surface plasmon resonance sensors are simple to function, provide real-time responses with high sensitivity and can be easily adapted for automation.[152] With respect to MIP-based plasmon resonance sensors, the binding interaction event that occurs between the analyte and imprinted receptor causes variation of the plasmonic wave at the metal-dielectric interface, producing a detectable signal.[153,154]

Cenci *et al.* synthesised a library of MIP nanoparticles (diameter 20–50 nm) targeting the N-terminus of the iron regulating hormone, Hepiciden-25, *via* precipitation polymerisation.[155] Sensitive and selective sensor response to the target hormone in spiked serum samples was detected within 180 s, using biotinylated MIP nanoparticles immobilised to

Table 3 Characteristics and performance of the e-nanoMIP sensor for multiple target detection. Reproduced with modifications from ref. 156, Copyright 2020 Springer Nature

Target	Glucose[a]	C4-homoserine lactone[a]	Paracetamol[b]	Tetrahydrocannabinol[b]	Trypsin[b]
Sensitivity	5.6 mA mM^{-1}	42 mA nM^{-1}	10.1 mA mM^{-1}	7.2 mA mM^{-1}	0.25 mA nM^{-1}
LoD	0.4 mM	0.1 nM	82 nM	50 nM	0.2 nM
Linear range	0.8–50 mM	6.2–800 nM	100–1000 mM	0.1–1000 mM	6.5–100 nM

[a] Tested in phosphate buffer saline. [b] Tested in human plasma.

a NeutrAvidin™ surface plasmon resonance sensor chip. Linearity was observed with the logarithm of Hepcidin-25 concentration in the range 7.2–720 pM, and LoD was calculated at 5 pM.[157] Recently reported micro-MIP-based surface plasmon resonance, at best, reached nanomolar sensitivities.[158–160] However, Cenci *et al.* highlighted biomarker detection on the picomolar level, credited to utilising completely polymeric MIP nanosized recognition elements integrated into surface plasmon resonance. Ultimately, these results demonstrate a viable approach for MIP integration into surface plasmon resonance for the identification of undetected peptides and proteins that have a fundamental role in pathogenesis but manage to elude existing means of detection.[155]

Garcia-Cruz *et al.* presented a generic electrochemical sensor platform, for a range of different targets, based on electro-responsive molecularly imprinted nanoparticles (e-nanoMIPs) for the potential employment of point-of-care diagnostics in the clinic.[156] This technology was applied to measure the concentration of targets including, glucose, trypsin, paracetamol, C4-homoserine lactone, and tetrahydrocannabinol, for the detection/monitoring of disease (*e.g.*, diabetes), biological molecules (*e.g.*, digestive enzyme), and drug conjugates for the design of affordable, robust, and disposable sensors.[156] The e-nanoMIP fabrication procedure involved controlled polymerisation of the monomer mixture (*e.g.*, methacrylic acid, ethylene glycol dimethacrylate, and trimethylolpropane trimethacrylate) in the presence of a specific target analyte immobilised onto an activated solid phase support (glass beads). A polymerisable ferrocene derivative was added to modify the standard composition of the prepared MIP.[156] Electrode modification relied upon well-established carbodiimide coupling of e-nanoMIP deposition onto the surface of a screen-printed gold electrode coated with self-assembled monolayers of alkanethiol.[157] Experimentally, all sensors demonstrated an electrochemical response time of 7 min, as shown by differential pulse voltammetry.[156,157] All e-nanoMIPs displayed a proportional increase in current response with respect to target analyte concentration (performance summary of each sensor is presented in Table 3), significant of sensitive and selective target detection. In essence, Garcia-Cruz *et al.* have developed a sensor fabrication process that can be exploited to assemble affordable, disposable, and transportable devices for microvolume sampling of a variety of target analytes present in biological media.[156,158]

Hong *et al.* utilised protein molecularly imprinting to fabricate a biomimetic sensor, exploiting the affinity of the C-reactive protein (CRP), an inflammatory protein, towards its natural ligand (phosphorylcholine).[13] The molecularly imprinted protein was synthesised in the presence of O-4-nitropehnylphosphorylcholine, polyethylene glycol 400 dimethacrylate and 2,2′-dimethoxy-2-phenyl-acetophenone, performing as functional monomer, crosslinker and initiator in a 1 : 4640 : 3.4 ratio, respectively, facilitating the formation of immuno-like membranes for the development of a microfluidic biochip for the rapid detection of the target protein (CRP). In this work, a point-of-care device for the separation and sensing of CRP from blood serum based on an immune-like polymer membrane (Fig. 6) was developed using well-orientated molecularly imprinted nanocavities.[13] The polymer membrane was integrated within a plastic microfluidic chip containing an enclosed interdigitated electrode array (Fig. 6a). The loading of human blood serum samples into the microfluidic biochip and the subsequent capture of the target protein by the protein imprinted recognition sites of the immuno-like membrane (Fig. 6b) was followed by the loading of sodium dodecyl sulphate and CRP release from the immuno-like membrane (Fig. 6c). This was proceeded by the final delivery of sodium dodecyl sulphate with the target protein to the electrodes (Fig. 6d) for electronic sensing based upon the rate of decay of the applied electric signal due to impedance changes. After initial incubation with spiked serum samples, CRP was detectable within 110 s. CRP was identifiable as low as 10 mg L^{-1}. Although this level surpasses the low to high-risk categories recommended for cardiovascular disease detection and is likely to be most beneficial for high-risk categories only, it is apparent from the dynamic response of the decaying signal that the approach of molecularly imprinted CRP selective cavities has the potential to detect lower CRP concentrations and form the basis for an improved clinically applicable biochip for point-of-care-testing.[159,160] Ultimately, the proposed approach is an adaptive technological platform, with the potential to facilitate cost-effective mass production for the application of a range of protein biomarkers.[13]

MIP-based biosensor capabilities towards detecting biological analytes within physiological fluids

Physiological media hosts a variety of biomarkers, and the biomarker concentration levels can give a detailed reflection of the status of human health.[161] The following section will discuss developments of MIP biosensors in their capability

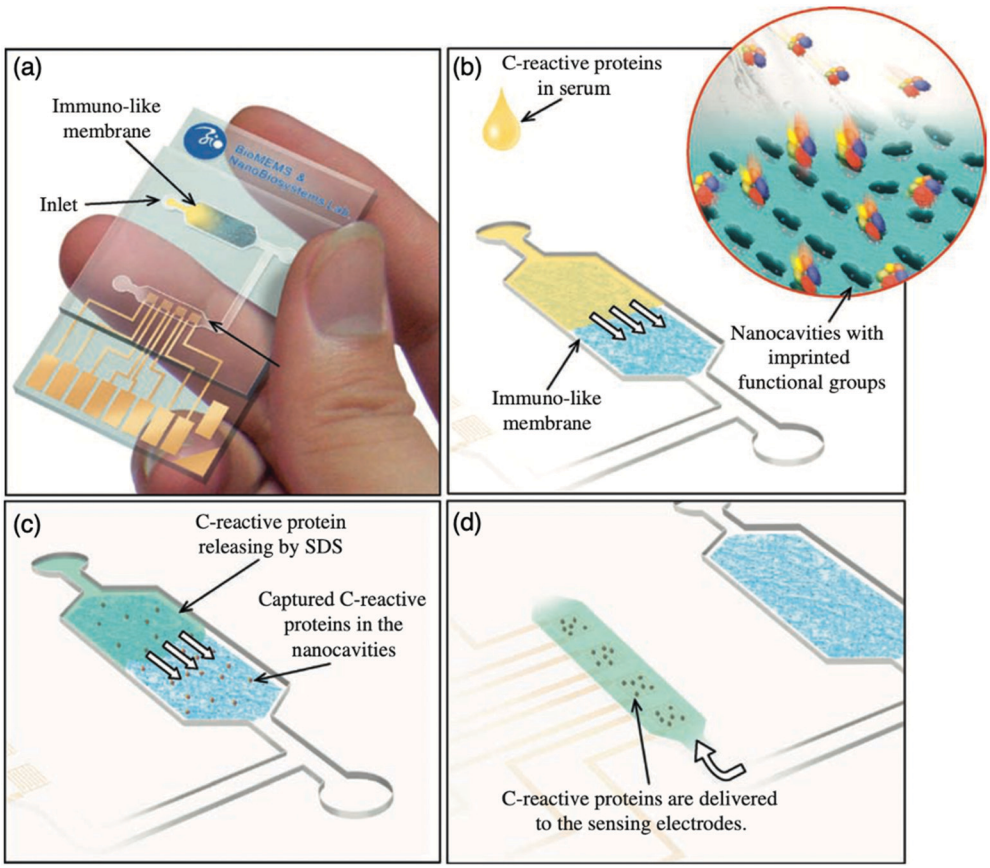

Fig. 6 Point-of-care sensing platform based on immuno-like membranes with molecularly aligned nanocavities for CRP detection. (a) Prepared membranes with aligned molecular nano-recognition for point-of-care protein biosensing. Immuno-like membrane in microfluidic biochip; (b) human blood serum sample loading and capturing of CRP; (c) loading of sodium dodecyl sulphate and releasing of CRP from the immuno-like membrane, and delivery of sodium dodecyl sulphate with CRP to the electrodes for electronic sensing. Reproduced with permission from ref. 13, Copyright 2013 Elsevier.

towards detecting biological analytes within a range of different biofluids.

Serum

Blood serum, the liquid left after blood clotting, exhibits many of the same solid components as plasma and is a popular biological fluid for disease detection, credited to its abundance of biochemical markers estimated at 250.[161] In turn, several recent works have focused on the detection of biomarker analysis within blood serum for the diagnosis of diabetes mellitus, liver cancer, human immunodeficiency virus, breast cancer, hypertryptophanemia, coronary heart disease, and many others.[134,162–165] You *et al.* utilised clinical blood serum samples for the detection of the amyloid-β oligomer, peptides responsible for the amyloid plaques present in Alzheimer brain lesions, *via* the fabrication of a novel electrochemical biosensor, where molecular imprinting was integrated with an aptamer-based sandwich assay as the sensor recognition unit.[166] Amyloid-β oligomer-specific aptamer was assembled onto the surface of the Ag/SiO_2 NPs *via* exploitation of the silver–thiol bond, establishing a Ag/SiO_2–aptamer bioconjugate. The molecularly imprinted layer was prepared with amyloid-β oligomer, methacrylic acid, divinylbenzene, and 2,2′-azo-bis-(2,4-dimethyl)valeronitrile performing as target analyte, functional monomer, crosslinker, and initiator, respectively.[166] Sensitivity was evaluated by measuring sensor response towards two variations of amyloid-β monomers, amyloid-β oligomers, and amyloid-β fibrils under identical conditions. Both variations of the amyloid-β monomers and amyloid-β fibrils showed a significantly weaker current response compared to that of the amyloid-β oligomers, credited to the specific recognition capabilities of the imprinted cavities installed *via* MIP and aptamer sandwich integration. Further investigation highlighted that different concentrations of the amyloid-β 1–42 oligomer showed a strong linear correlation ranging between 5 pg mL^{-1}–10 ng mL^{-1} (R^2 = 0.997), where the LoD was calculated at 1.22 pg mL^{-1}.[166] Thus, the response of the biosensor correlates to an amyloid-β oligomer concentration range within the detection range found in physiological serum of Alzheimer's disease patients (1.35–12.5 ng mL^{-1}).[167]

The preparation of 12 amyloid-β 1–42 MIP biosensors under identical conditions demonstrated a relative standard deviation (RSD) value of 7.7% for the detection of 1 ng mL^{-1} of amyloid-β

1–42 oligomer, indicating that the MIP could be reproduced satisfactorily. Stability was monitored by measuring the electrochemical signal of the sensor every week, where ~91.2% of the original signal intensity was retained after 28 days. Recovery of the amyloid-β 1–42 oligomer from spiked healthy human blood serum samples ranged between 93–107.7% with acceptable RSDs ranging from 2.5 to 9.8%, verifying the applicability of the fabricated MIP biosensor for amyloid-β1–42 oligomer determination in clinical samples for early Alzheimer's disease diagnosis.[171]

Jaiswal *et al.* reported a MIP-based electrochemical sensor developed *via* a layer-by-layer approach, capable of quantitatively differentiating between ultra-trace levels of D- and L-serine in blood serum and cerebrospinal fluid of clinical patients.[168] Serine, has a crucial role in the functioning of the central nervous system, and is a biomarker of psychiatric disorders (*e.g.*, schizophrenia).[169] Imprinted polymeric films were comprised of acrylamide, copper(II) oxide, 2,2′-bipyridine, and chloroform, acting as functional monomer, catalyst, ligand, and initiator, respectively. Layer-by-layer assembly was achieved by grafting synthesised imprinted polymeric films *via* spin coating on the surface of pencil graphite electrodes. Jaiswal *et al.* prepared a highly sensitive biosensor, with respect to other biosensors evaluating the same target analyte, inferred by a 0.24 ng mL^{-1} and 0.25 ng mL^{-1} LoD for D-serine (0.83–20.63 ng mL^{-1} LoD range) and L-serine (0.87–20.45 LoD range), respectively (inclusive of both biological fluids), utilised for sequential analysis of isomeric target analytes using a single electrode.[170–175] The authors reported that the artificial recognition component, (*i.e.*, the MIP), presented an *IF* of 25.61, absent of any regeneration limitations, cross-reactivity, and false positives, highlighting its capability to improve medical diagnostics for the correct management of administered medications and facility admittance.[168]

Luo *et al.* developed a magnetic surface molecularly imprinted-resonance light scattering sensor for the rapid and highly sensitive detection of the Japanese encephalitis virus (JEV), a mosquito-transmitted virus that can cause inflammation of the brain.[176,177] The surface imprinted polymer was prepared on silicon-coated iron oxide microspheres and polymerisation was performed using aminopropyltriethoxysilane and tetraethyl orthosilicate as functional monomer and cross-linker to immobilise the target virus (JEV) and secure the three-dimensional polymeric network, respectively. The sensitive and selective detection of JEV was initially determined in Britton–Robinson buffer. Under optimised conditions, the LoD was observed at 1.3 pM (3.0%, RSD).[176] In comparison to previously reported MIP optical sensors for the detection of JEV, the detection limit (1.3 pM) is clinically acceptable, and sensor response time (20 min) is significantly faster.[176–179] The response of the magnetic MIPs towards JEV in the presence of other viruses, including Hepatitis A virus, dimensionally different Rabies virus, and Simian vacuolating virus 40, using an initial virus concentration of 75 ng mL^{-1}, showed that the imprinted JEV could be selectively detected with low non-specific adsorption when in the presence of virus interferents. The feasibility of the prepared MIP-sensor for the detection of JEV in clinically relevant samples was examined in spiked (10–90 ng mL^{-1}) healthy human serum samples. Sensing performance was ascribed by recovery rates ranging between 98.0–110.2%, suggestive of the designed approach being a promising means to detect the target virus in patient samples.[176]

To address drawbacks of using antibodies for cancer biomarker recognition, Tawfik *et al.* utilised optical methods in the form of fluorescent molecularly imprinted conjugated polythiophenes to develop a simple and affordable enzyme-free amplification assay for the detection of α-fetoprotein, a biomarker of liver cancer, undetectable among healthy individuals, within blood serum samples.[185] This strategy relied upon dual emission fluorescent molecularly imprinted conjugated polymers (MICPs) fabricated with specific α-fetoprotein and carcinoembryonic antigen affinity and enhanced fluorescence features (Fig. 7). Signal amplification was generated by exploiting two varying conjugated polymers green- and yellow-emitting polythiophenes, where photoluminescence quantum yield was observed at 35% and 55%, respectively. Both imprinted species were synthesised *via* ultraviolet chemical polymerisation (λ = 365 nm), where conjugated polythiophenes were solubilised in 4-vinylphenylboronic acid in the presence of the target analyte, polyethylene glycol dimethacrylate (crosslinker), and 1-hydroxycyclohexyl phenyl ketone (photo initiator).[180] Initial α-fetoprotein sensitivity parameters were examined in phosphate-buffered saline, where a LoD of 2.50 pg mL^{-1} and 1.20 pg mL^{-1} for green- and yellow-emitting fluorescent MIPs, respectively, was recorded.[180] Comparatively, the obtained LoD values showed improvement with regard to state-of-the-art α-fetoprotein biosensors.[181–189]

The designed sensor's feasibility was surveyed in multiple human physiological fluids. Traces of α-fetoprotein in human blood serum were analysed, where LoDs for green- and yellow-emitting MICPs were valued at 5.0 pg mL^{-1} and 2.2 pg mL^{-1}, respectively. For saliva samples, LoDs were calculated at 2.1 pg mL^{-1} and 1.1 pg mL^{-1} for green- and yellow-emitting MICPs, respectively. Attained values agreed with early α-fetoprotein detection in clinical samples, where the onset for positive results is 5 ng mL^{-1}. In addition, target recovery from α-fetoprotein spiked blood serum varied between 98.9–110% (1.56–3.65%, RSD) and 98–105% (1.88–3.66%, RSD) for green- and yellow-emitting MICPs, respectively. For saliva samples, recovery ranges included 96.90–110% (1.91–4.21%, RSD) and 97.30–110% (2.43–3.66%, RSD) for green- and yellow-emitting MICPs, respectively.[185]

As a proof of principle, the designed MIP sensors were used for α-fetoprotein analysis of clinical blood serum provided by liver cancer patients. The quantified α-fetoprotein concentrations from both MIP biosensor assays were concurrent to those probed by enzyme-linked immunosorbent assay (ELISA) analysis, reflected by high linear correlations (R^2 = 0.985 and R^2 = 0.987, respectively). Therefore, Tawfik *et al.* has unveiled a pioneering step to advance universally accessible, affordable, portable, point-of-care cancer diagnostics using optical MIP

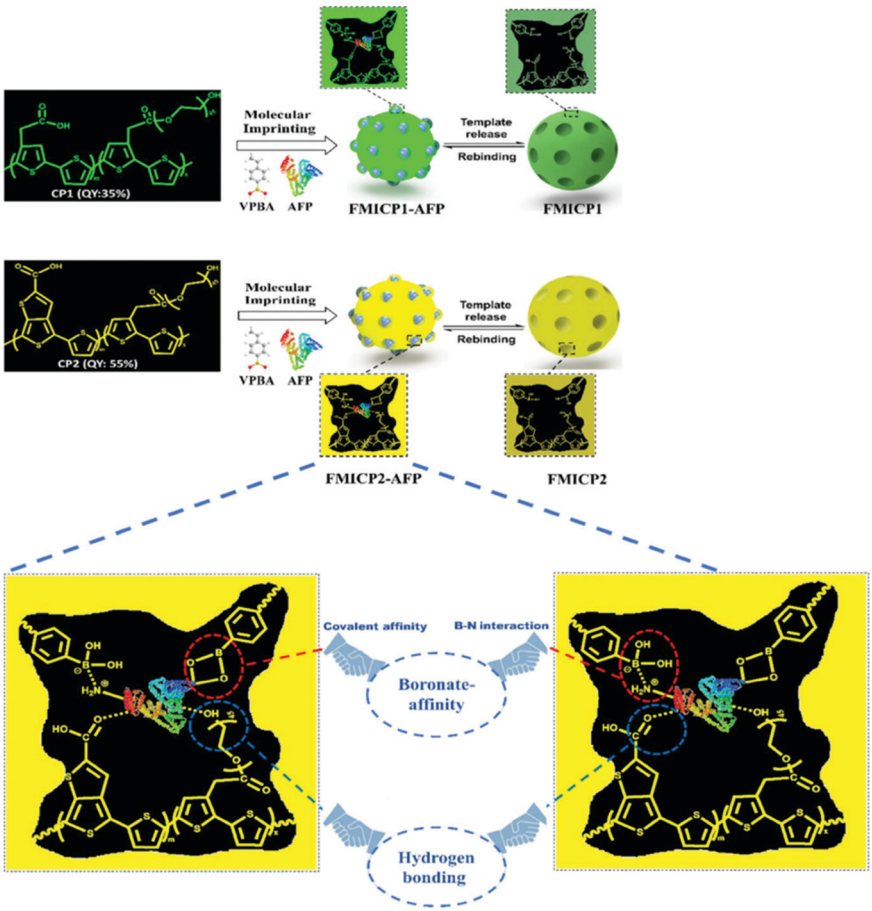

Fig. 7 A dual emission non-ionic molecular imprinted conjugated polythiophene-based paper device for α-fetoprotein detection. Mechanistic insight into dual-emission conjugated polymers linked with boronate-affinity molecular imprinting technique. Reproduced with permission from ref. 180, Copyright 2020 Elsevier.

biosensors in physiological samples, which will be of significant benefit in resource-limited clinical settings.[180]

Saliva

Unlike serum, saliva sampling is non-invasive, with significantly less risk of subsequent infection (from possible needle contamination) and overall cost.[190] Furthermore, salivary biomarker detection is becoming a popular method for diagnostics, credited to its accessibility of biological analytes associated with disease, common to those found in human blood.[134,137,191–195] Diouf *et al.* capitalised on this biofluid *via* the development of a MIP electrochemical sensor for the sensitive detection of glucose in saliva.[196] Healthy physiological salivary and blood glucose levels range between 0.05–21.61 mg dL^{-1} and 70–120 mg dL^{-1}, respectively.[196] Despite the very selective, specific and sensitive nature of enzymatic glucose sensors, their applications are hindered by their complexity, lack of stability, limited operational conditions (*e.g.*, temperature, pH, and humidity sensitivity, refer to Table 1), and heavy reliance on blood samples from finger-pricking.[197,198] Despite these issues, there are minimal reports focused on non-enzymatic biosensors for the direct detection of glucose; therefore, there is a gap in the current clinical commercial market for the development of a non-invasive and effective glucometer for continuous, accurate, and rapid measurements.[199]

In response to the current commercial limitations, Diouf *et al.* fabricated a non-enzymatic MIP sensor based on electrochemical polymerisation of the functional monomer acrylamide cross-linked by *N*,*N*′-methylene bis-acrylamide in the presence of glucose onto a gold surface printed electrode to determine glucose concentrations in real saliva samples (Fig. 8).[196] Electrochemical detection of glucose within a working range of 0.5–50 μg mL^{-1} was achieved by introducing the working electrode into a known concentration of glucose. A ferricyanide redox probe was utilised to monitor decreasing current in response to increasing glucose concentration, explained by the binding of glucose molecules with that of MIP recognition cavities - impeding electron transport to the redox probe. Differential pulse voltammetry and electrical impedance spectrometry were utilised to determine the LoD, reported at 0.59 μg mL^{-1} and 1.6 μg mL^{-1}, respectively. Notably, the NIP species showed a negligible change of signal, signifying that observed responses directly resulted from the immobilised glucose within imprinted glucose cavities.[196] The selectivity of this glucose MIP sensor was measured using lactose and sucrose, two interfering analytes, naturally coexisting in biological saliva samples, with a similar

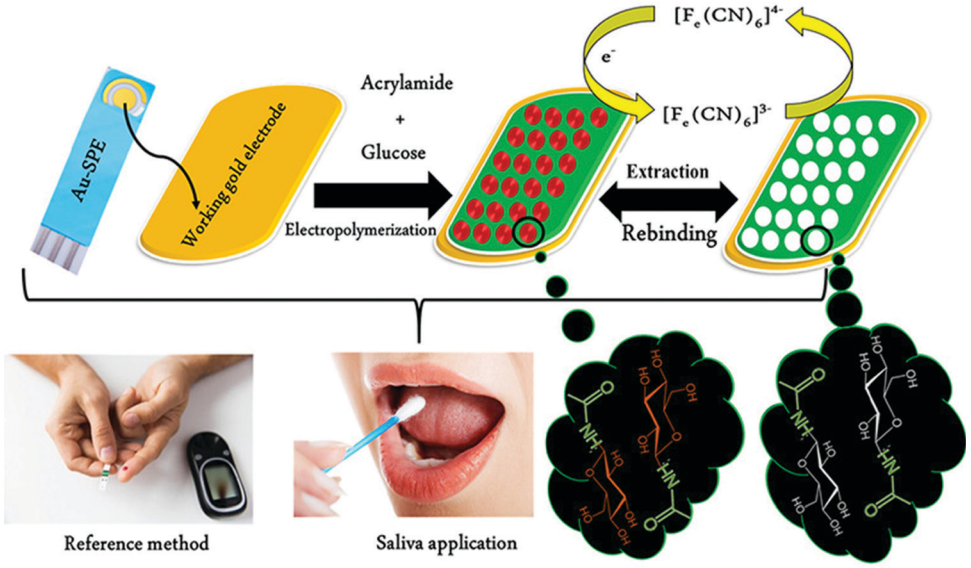

Fig. 8 Fabrication of a MIP-based screen-printed gold electrode (Au-SPE) for the diagnosis of diabetes mellitus prepared in the presence of glucose as the template, where the binding sites of molecular interactions have been highlighted. Traditional methods of finger-prick blood sampling have been presented as a comparison to emphasise the ease and pain-free means of saliva sampling. Reproduced with permission from ref. 196, Copyright 2019 Elsevier.

structure to that of glucose. No significant response was obtained from either interferant. Thus, the proposed glucose MIP sensor showed a remarkable selectivity towards glucose molecules only. Additionally, the reproducibility (3.4%, RSD), repeatability (4.0%, RSD), and stability (retained 85% of its initial response) of the MIP sensor were also investigated, where stability was monitored at regular time intervals over a three-month period.[196] The fabricated glucose MIP sensor was applied to saliva samples of six healthy volunteers. Sampling procedures involved mouth rinsing followed by storage at 4 °C. Saliva glucose levels were compared to that of finger-prick blood. Salivary glucose and fasting blood glucose values ranged between 0.22–0.86 mg dL^{-1} and 94–147 mg dL^{-1}, respectively. Consequently, Diouf *et al.* have established an inexpensive, simple, and effective sensing platform for non-enzymatic glucose detection, assembling a promising tool for the future evolution of accurate and reliable non-invasive diabetes mellitus diagnosis using MIT. To further validate the obtained results within this study, additional data should be collected from saliva samples of diabetic patients.[201]

Salivary biomarker analysis was also adopted by Parnianchi *et al.*, who recently developed, for the first time, a highly sensitive and selective electrochemical sensor integrated with a MIP for the detection of bilirubin.[200] Bilirubin is a metabolite of the catalytic degradation of heme in haemoglobin and can be utilised as a biomarker of anaemia (low levels) and liver disease (high levels).[201–203] Due to the electrochemical applications of multi-walled carbon nanotubes, these structures were used to modify the electrodes prior to *o*-phenylenediamine (functional monomer) electropolymerisation in the presence and absence of bilirubin for MIP and NIP electrode preparation, respectively.[200,204]

Preceding biosensor employment for the detection of bilirubin in real human samples, the sensing platform was first characterised using ferricyanide as an electrochemical probe. Analyses highlighted that when the target analyte was removed from the polymer film, there was a significant decrease in electron transfer resistance, credited to the successful imprinting of bilirubin cavities performing as electron transfer channels – reducing resistance. Ultimately, modified MIP electrodes showed a wide linear range of 12.08–91.81 fM with a 7.8 fM LoD.[200] Sensor selectivity was investigated *via* structurally similar analogues to bilirubin, including progesterone, testosterone, dopamine, uric acid, and ascorbic acid. Each structure was examined three times and signified negligible cavity adsorption compared to the bilirubin template, valuing MIP sensor selectivity at 1.05 μA fM^{-1}.[200] Furthermore, this MIP electrode signified reasonable operational stability (*i.e.*, it can be used several times), attributed to a minimal 5% signal loss over a period of 10 days, which is in agreement with other reported studies.[205–208] Following optimisation testing, the selective detection of bilirubin in human saliva of neonates and adults, was analysed. Samples relating to healthy adult saliva were prepared in different concentrations ranging from dilution factors of 0–1000. MIP sensor performance was examined by the addition of standard bilirubin in the femtomolar range (12.08–91.81 fM), where clinically reasonable responses were observed as identified by an average bilirubin recovery of 97.41% with an RSD of 3.84 ($n = 4$). However, detection of bilirubin from the samples relating to infants with symptoms of jaundice using the developed MIP sensor showed a decrease in target analyte recovery (95.9% with an RSD of 6.0% ($n = 4$)) when compared to results obtained using high-performance liquid chromatography (HPLC).[200]

Cerebrospinal fluid

In contrast to saliva, cerebrospinal fluid sampling is a more invasive technique. Cerebrospinal fluid is an invaluable clinical specimen that offers critical information regarding diseases,

infections, and severe conditions affecting the spinal cord and brain.[209–211] Ji *et al.* fabricated a MIP monolith using a micropipette tip, prepared *via* epitope imprinting, for the highly selective extraction of cholecystokinin neuropeptides (Fig. 9).[212] Cholecystokinin neuropeptides are active within the physiological and pathophysiological processes of the central nervous system, contributing to mental health disorders (*e.g.*, schizophrenia) and epilepsy; therefore, the development of accurate analytical techniques within the fluid is vital.[213,214]

The designed MIP monolith exhibited specific recognition capability, high cholecystokinin neuropeptides (CCK) recapture capacity, and excellent reusability. Initially, *in situ* polymerisation occurred, where methacrylic acid, ethylene glycol dimethacrylate, and 2,2′-azobisisobutyronitrile were applied as functional monomer, crosslinker, and initiator, respectively, in the presence of the template CCK4. Template extraction revealed imprinted cavities that could selectively recognise CCK4 and structurally similar CCKs (*i.e.*, species that shared the same imprinted amino acid sequences), including CCK5 and CCK8. In addition, three oligopeptides, including tetrapeptide, Leu-enkephalin and Met-enkephalin, were introduced to interfere with the specific binding observed for the CCK neuropeptides for sensor selectivity evaluation. Nonetheless, the MIP monolith demonstrated a significant molecular affinity and selectivity enrichment capability for CCK neuropeptides only.[212] Sensor applicability was determined by monitoring CCK neuropeptide in clinical human cerebrospinal fluid samples. Formulated calibration curves for CCK4 (R^2 = 0.981) and CCK8 (R^2 = 0.973) signified LoDs calculated at 1.2 and 5.5 pM, respectively. Linearity and target recoveries (73.9–90.4%) were within clinically acceptable limits. The feasibility of the prepared MIP monolith sensor has shown that with the combination of sample purification and enrichment, it was possible to detect CCK neuropeptides in cerebrospinal fluid at physiological levels.[212]

Luliński *et al.* developed a MIP to detect tryptamine within cerebrospinal fluid to monitor cardiovascular pathologies (*e.g.*, myocardial infarction, hypertension). The sensor was fabricated *via* molecularly imprinted solid-phase extraction (MISPE) and HPLC combined with fluorometric signal technology. The tryptamine-imprinted microscale sorbent (stationary phase), performing as sensor recognition, was synthesised *via* both bulk and precipitation polymerisation, where 4-vinylbenzoic acid and ethylene glycol dimethacrylate were employed as functional monomer and crosslinker, respectively. Static (sensitivity determination) and dynamic experiments (selectivity determination) revealed an *IF* of 15.4 and 18.62, respectively. Tryptamine determination in the presence of serotonin and L-tryptophan was validated using a complex matrix of bovine serum albumin yielding the recoveries of tryptamine that ranged between 98.7 and 107.0% (1.1–3.7%, RSD).[215] Human cerebrospinal fluid (post-mortem) was then tested to determine the practicality of the MIP sensor in the presence of competitors. First, the elution fraction obtained from pure cerebrospinal fluid was spiked with standards of tyramine (1.31),

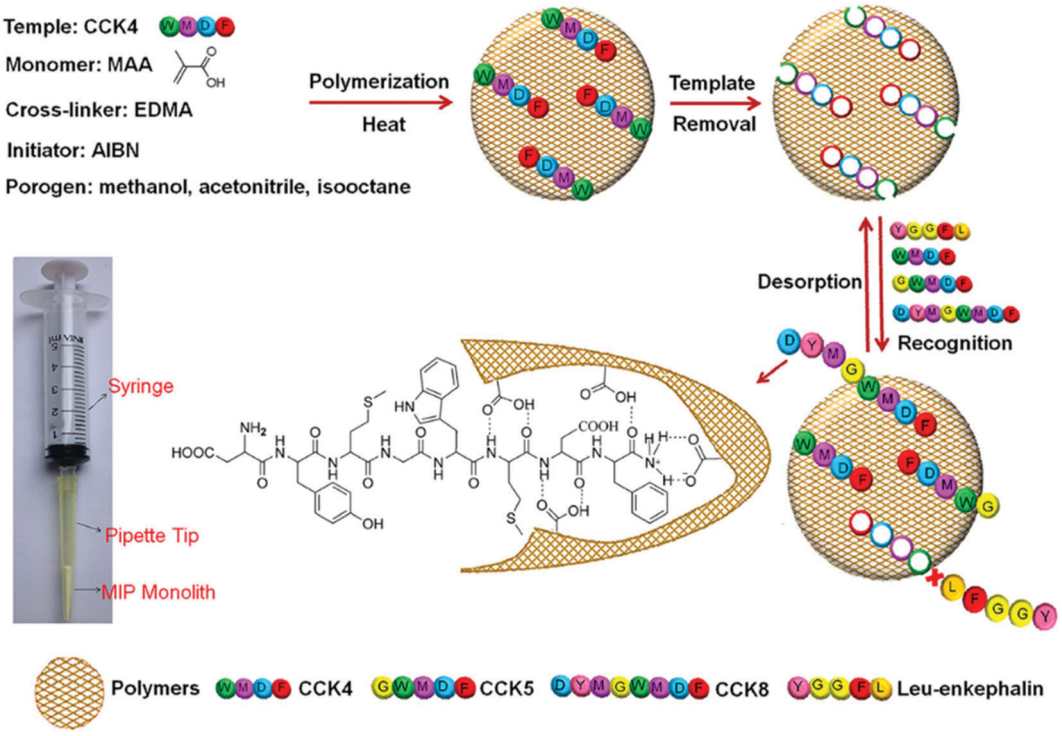

Fig. 9 Schematic depiction of the MIP monolith fabrication protocol for the selective recognition of cholecystokinin (CCK) neuropeptides in cerebrospinal fluid. The monomer and template interactions are highlighted. A micropipette tip connected to a syringe is utilised to perform the molecularly imprinted solid-phase microextraction (MI-μ-SPE) for the detection of CCK neuropeptides *via* the epitope imprinting approach. Reproduced with permission from ref. 212, Copyright 2015 John Wiley & Sons.

serotonin (*IF* = 1.21), and L-tryptophan (*IF* = 1.16) to identify the presence of eluent interferants. The Q_{max} of tryptamine (186 ± 19 mmol g^{-1}) is greater than that of the interfering species (15.9 ± 1.6, 39.9 ± 4.0, and 117 ± 12 mmol g^{-1}, respectively), indicative of MIP target adsorption. The reported values are explained by structural analogy to that of tryptamine, as the interferants all share a similar indole ring with an ethylamine aliphatic chain. Nevertheless, the MIP sensor clearly demonstrates tryptamine selectivity irrespective of the present interferants. All signals were achieved in <15 min. Neat human cerebrospinal fluid spiked with the internal standard (5-methoxy-tryptamine) was also tested for extraction processes to quantify the concentration of tryptamine in the eluent. All signals were achieved in <25 min. Ultimately, MISPE techniques demonstrated a very low tryptamine LoD (19.9 nmol L^{-1}) in bovine serum albumin, and tryptamine was also quantified in human cerebrospinal fluid (553 ± 45 nmol L^{-1} (n = 3)), even in the presence of competitive structural equivalents. Thus, the authors have developed a novel analytical procedure to determine tryptamine in real human samples for a better-magnified insight into cardiovascular-related ailments.[215]

Sweat

Sweat has a less complicated matrix than other physiological fluids, resulting in the secretion of metabolites in an acidic and electrolyte-rich fluid.[216] The minimally invasive nature and easy collection of this fluid due to several accessible sampling sites enables sweat to be used in applications for continuous analysis.[217] Recently, Mugo *et al.* utilised this media to develop a molecularly imprinted cortisol selective biosensor, fabricated *via* the layer-by-layer assembly for elevated cortisol detection, implicated in various stress-related conditions (*e.g.*, post-traumatic stress disorder and bipolar disorder).[218,219] As such, cortisol can be a valuable biomarker for diagnosing physiological conditions related to anxiety, depression, and mental health.[220] The sensor layers comprised a stretchable polydimethylsiloxane base with carbon nanotube-cellulose nanocrystals (CNC/CNT) conductive nanoporous nanofilms. The MIP was fabricated *via* surface imprinting using glycidyl methacrylate (functional monomer) and ethylene glycol dimethacrylate (crosslinker) where is was deposited onto the CNC/CNT, forming the cortisol biomimetic receptor.[218]

Sensitivity of the MIP was shown by a 180 s sensor response, with a 2.0 ± 0.4 ng mL^{-1} LoD (2.6%, RSD) to cortisol in phosphate buffer, attributed to the inherent receptor-specific cavities engrained in the MIP film.[221] Increasing cortisol concentrations yielded a linear calibration (R^2 = 0.92) with a high calibration sensitivity four orders of magnitude higher than the NIP, acting as a control. Moreover, the MIP cortisol sensor dynamic range was determined to be 6–60 ng mL^{-1}, falling within the physiological cortisol range (8–50 ng mL^{-1}) in human sweat, thus confirming the feasibility of the prepared sensor for cortisol detection in biological sweat.[217] Although former reported cortisol biometric sensors have displayed lower LoD values; these sensors rely on antibodies.[222–224] Specificity of the imprinted cortisol sensor was determined *via* analysis of analogous interfering chemical species, similar to those already present in human sweat. The interfering species tested included epinephrine, methoxyxprogestone, β-estradiol and glucose. The MIP sensor exhibited high specificity towards cortisol with a measurable difference in voltammetric readings, compared to the introduction of the other interfering species.[218] Biosensor feasibility was evaluated for *ex situ* analysis of sweat samples. Following triplicate measurements, cortisol concentration was determined to be 33 ± 2 ng mL^{-1} (5.4%, RSD), which falls within the normal clinical range. The MIP sensor's cortisol content was also validated by HPLC, resulting in a very similar concentration of 29 ± 0.5 ng mL^{-1} (5%, RSD).[218]

In a recent study, Tang *et al.* developed a touch-based MIP biosensor (Fig. 10a) for selective cortisol detection through natural perspiration. Instead of sweat sampling *via* stimulative methods (*e.g.*, exercise), this sensor was designed to measure fingertip sweat cortisol through touch *via* highly selective binding to the cortisol-imprinted electropolymerised polypyrrole coating, where Prussian blue was embedded as the redox probe. The high density of eccrine sweat glands present in the fingers can produce high sweat volumes, which can subsequently be collected by the highly porous, permeable, and sweat absorbing polyvinyl alcohol hydrogel. Thus, this MIP-based fingertip cortisol biosensor has generated a natural and practical sweat sampling technique, providing a stressless, label-free, low-cost point-of-care testing platform for mental health management and monitoring, exemplifying a potential step-change in the disciplines of wearable biosensor devices and personalised healthcare.[225]

Zhang *et al.* developed a wearable electrochemical biosensor by incorporating silver nanowires and a MIP electropolymerised in the presence of 3-aminophenulboronic acid (functional monomer) on a screen-printed electrode for the non-invasive monitoring of lactate in human sweat.[226] During exercise, sweat lactate concentrations can ascend to 25 mM; however, a severe imbalance can lead to anaerobic metabolism (*e.g.*, pulmonary embolism or haemorrhagic shock).[227,228] The MIP sensor exhibited high sensitivity and specificity for the detection of lactate in phosphate buffer saline from 10^{-6}–10^{-1} M, significant of a 22 μM LoD. Furthermore, the sensors had high stability and reproducibility with a sensitivity recovery of 99.8% ± 1.7% seven months after being stored in the dark at room temperature. Glucose, urea, pyruvic acid, uric acid, sodium chloride, calcium chloride and ammonium hydroxide were among the many substances utilised to measure the sensor's selectivity, primarily due to their structural resemblance to the metabolic substances found in human sweat. Generally, the sensor response showed good selectivity towards the target and negligible response to the interferants. Urea, pyruvic acid and uric acid give the highest current changes around 3 × 10^{-7} A, which is only 1.4% of the specific response for lactate (14 mM) binding (2.2 × 10^{-5} A).[226] Epidermal lactate measurements were performed on six healthy volunteers. A thin film of polydimethylsiloxane with a sweat cell was utilised for the upwards attachment of the electrode biosensor to the volunteer's skin, enabling sweat overflow after cell saturation (Fig. 10b). Differential pulse voltammetry responses were recorded every five minutes for a period of 30 minutes during exercise. After

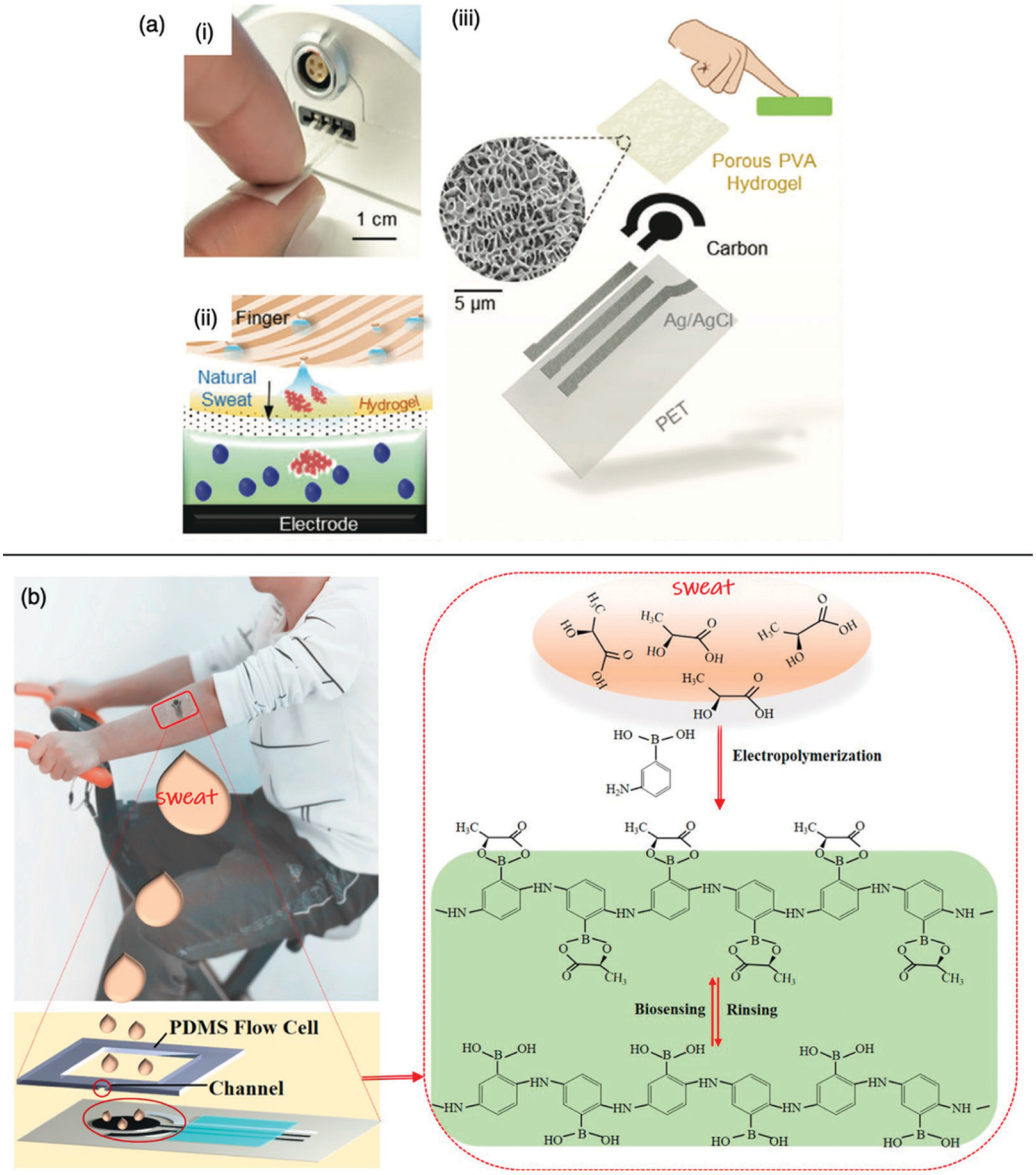

Fig. 10 Molecularly imprinted sweat sensors for healthcare monitoring. (a) Cortisol-imprinted electropolymerised polypyrrole-based sensor for the rapid and stressless detection of cortisol (i) The touch-based cortisol biosensor demonstrating the single-touch application; (ii) sensing mechanism illustration describing the cortisol accumulation from finger sweat diffusing through the hydrogel onto the MIP electrode; and (iii) a structural depiction of the sensor with cryogenic scanning electron microscopy image of the porous hydrogel. Reproduced with permission from ref. 225, Copyright 2021 John Wiley & Sons. (b) Molecularly imprinted silver (Ag) nanowires for the detection of lactate. Application of the designed screen-printed three-electrode biosensor chip to a human volunteer for the feasible determination of sweat sensing during exercise exertion, where the binding principle of the MIP biosensor fabrication and sensing process is highlighted. Reproduced with permission from ref. 226, Copyright 2020 Elsevier.

10 minutes of exercise, skin moisture became evident, and the differential pulse voltammetry current began to show a reduction, resulting in sweat lactate build-up. After 30 minutes of exercise, a sweat lactate concentration of 14 mM was measured. The same MIP silver nanowires biosensor was then applied to the remainder of the volunteers, producing parallel current responses validating the MIP device reconcilability. Ultimately, the described epidermal biosensor showed a higher sensitivity for lactate concentrations through an easily accessible medium, as opposed to many other lactate biosensors, offering on-body monitoring of perspiration lactate for real-time monitoring of human health conditions.[231]

Urine

Urine can also provide real-time monitoring for biomarker studies, as highlighted by multiple reports based on the construction of MIP-based biosensors for urine analysis.[138,211,229,230] Zhang *et al.* produced a MIP-based electrochemical biosensor supported by a dual-signal technique to evaluate human serum albumin in real urine samples.[231] Urine albumin excretion,

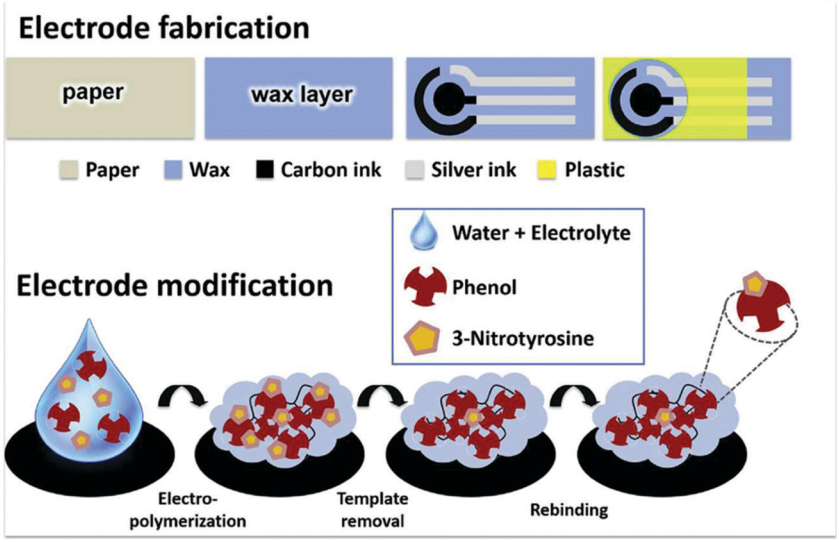

Fig. 11 Illustrative depiction of a paper-based electrode. Electrode modification occurs *via* molecular imprinting of the 3-nitrotyrosine template, formulating a sensor film receptive of the template molecule. Reproduced with permission from ref. 237, Copyright 2020 Elsevier.

a bulky negatively charged protein, can indicate early-stage chronic nephritis, diabetes, and endothelial dysfunction.[232] Sensor fabrication was achieved by modifying a glassy electrode substrate with gold nanoparticles and polythionine-methylene blue, displaying a MIP film synthesised *via* electropolymerisation using *o*-phenylenediamine and hydroquinone as functional monomers. Sensitivity was observed within the linear range of 10^{-10}–10^{-4} g L^{-1} (R^2 = 0.995) by simultaneously decreasing substrate and solution probe peak currents, indicative of human serum albumin occupied imprinted cavities (3×10^{-11} g L^{-1}, LoD).[231] Notably, the designed sensor demonstrated lower LoD values when compared with other published MIP-sensors specific for human serum albumin detection.[210,229,231,233–236] The biosensor exhibited reasonable sensor selectivity when tested with a range of competitive substances, including glycine, glutamate, cysteine, tryptophan, histidine, dopamine, ascorbic acid, haemoglobin, and bovine serum albumin. The biosensor also demonstrated reproducibility (4.4%, RSD (n = 5)) and stability at 95.3% of initial signal retention. The MIP sensor applicability was evaluated by measuring target protein concentrations from urine samples of an unwell patient and a healthy volunteer, where serum albumin recovery varied between 90–104% (3.0–3.5%, RSD) and 95–105% (2.2–3.9%, RSD), respectively. These values concur with the immunoturbidimetry assay results from the hospital record, suggesting that the proposed biosensor proposed promising results for clinical assays.[231]

Martins *et al.*, like Tawfik *et al.*, developed a paper-based biosensor, encouraging improved affordability, sustainability, and reliability of support materials for the design of point-of-care diagnostic devices. A label-free detection method involving direct MIP assembly on a paper platform, integrated with a conductive carbon ink for suitable electrochemical transduction, was incentivised for the recognition of 3-nitrotyrosine in urine. 3-Nitrotyrosine is an important marker for oxidative stress, responsible for neurodegenerative disorders (*e.g.*, Alzheimer's and Parkinson's disease). The MIP film was deposited on the surface of the carbon-coated electrode through bulk polymerisation, followed by electropolymerisation using phenol as a functional monomer (Fig. 11).[237] 3-Nitrotyrosine concentrations were monitored *via* the immersion of the MIP-based device in spiked human urine samples. A linear correlation for both the MIP and NIP (control) species was observed for 3-nitrotyrosine concentrations ranging between 5 μM–1 mM; however, the MIP sensor demonstrated greater linear sensitivity (R^2 = 0.994), reproducibility (smaller error bars) and an LoD of 22.3 nM (1–2%, RSD (n = 3)).[237] In comparison to previously reported works involving MIPs coupled with electrochemical sensing that were amplified using nanomaterials, this reported LoD is clinically viable.[242]

Nasopharyngeal fluid

The COVID-19 pandemic has highlighted the importance of point-of-care testing using safely accessible physiological media, such as nasopharyngeal fluid. Although remarkable progress has already been achieved, there is still great demand for simple and rapid diagnostic tools for the early detection of the coronavirus disease. Molecular assays, *i.e.*, real-time polymerase chain reaction (RT-PCR), have become the gold standard for accurate severe acute respiratory syndrome coronavirus 2 (SARS-CoV-2) detection.[238] Unfortunately, due to the time-consuming analysis, instrumentation costs, and the need for medically trained personnel, the use of RT-PCR can be limited.[239–241] Consequently, there is still an urgent need for more affordable, portable and sensitive devices for COVID-19 diagnostics.

Commercially available point-of-care diagnostic tools for the detection of the SARS-CoV-2-specific antigens, such as the qualitative lateral flow immunochromatographic assays, utilise the antibody-based detection principle, producing results within 15–30 min.[242] Alternatively, point-of-care diagnostic

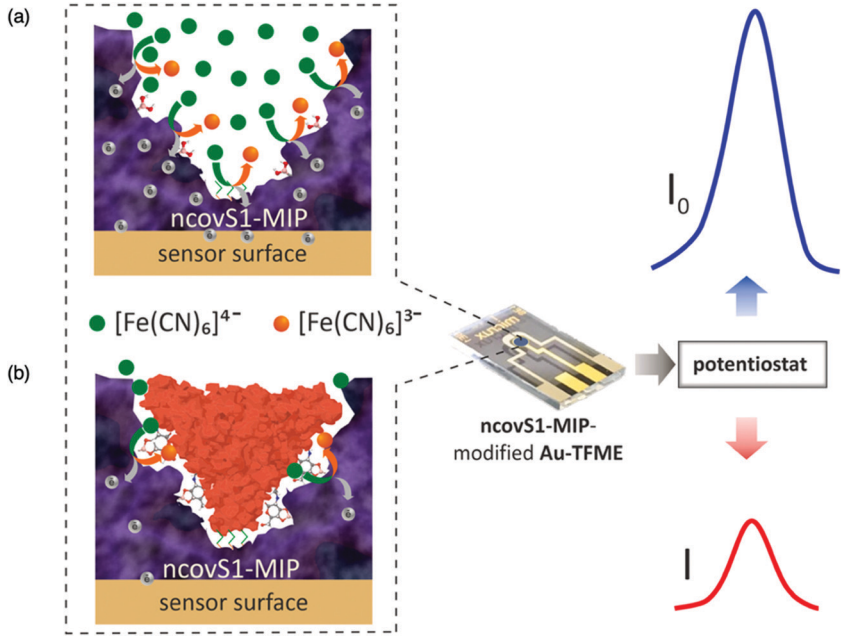

Fig. 12 The operating principles of the developed coronavirus detecting device for the sensitive and selective detection of ncovS1 and ncovNP, respectively. (a) Redox probe readily carrying the charge through the ncovS1-MIP producing current (I_0); (b) the rebound ncovS1 blocks pathways for the redox probe to carry the charge through ncovS1-MIP, leading to a concentration-dependent contraction in the recorded current (I). Reproduced with permission from ref. 245, Copyright 2022 Elsevier.

tools based on electrochemical sensing platforms have also been reported.[243,244] Nevertheless, current forms of coronavirus detecting systems suffer from special storage systems to preserve their shelf life due to the environmental sensitivity of the biological materials.[245]

Ayankojo and co-authors have recently developed a MIP-based electrochemical sensor for the quantitative detection of the SARS-CoV-2 spike protein subunit S1 (ncovS1) found in the nasopharyngeal fluid of coronavirus patients for the rapid detection of coronavirus disease.[245] The authors exploited the covalent interaction between 1,2-diols of the highly glycosylated protein and the boronic acid group of 3-aminophenyl-boronic acid (functional monomer). A disposable thin-film gold electrode chip was modified with a MIP film with selectivity toward the ncovS1, acting as the recognition element (Fig. 12a and b).[245]

Clinical samples consisted of nasopharyngeal specimens of three negative and five positive coronavirus patients in sample preservation solution, where their coronavirus status was previously confirmed *via* RT-PCR. The fabricated sensor displayed a reaction and measurement time of 15 and 5 min, respectively. Device sensitivity towards ncovS1 detection in nasopharyngeal samples showed a LoD of 4.8 pg mL^{-1} (linear range of 0–30 pg mL^{-1}).[245] When compared to other electrochemical sensor platforms for SARS-CoV-2 detection reported in the literature, the ncovS1 sensor presented a clinically reasonable performance with improved rapid results output.[244,246–249]

The selectivity of the sensor was determined by spiking negative coronavirus samples with varying concentrations of either ncovS1, SARS-CoV-2 nucleo-protein (ncovNP) or their mixture. The responses induced on the sensor by the increasing concentration of ncovNP were below the LoD, indicating no recognition for ncovNP, whereas increasing responses above the LoD were seen towards ncovS1. Furthermore, the responses induced by the mixture of both proteins in a 1 : 10 ratio are comparable to that from ncovS1, thus, indicating that the presence of ncovNP in the sample does not interfere, to any significant extent, with the sensor-specific recognition of ncovS1 thereby enabling its accurate analysis.[245]

The proposed strategy has established its suitability as a potential diagnostic tool for clinical assessment of SARS-CoV-2, demonstrating a substantial quantitative advantage apropos to the LoD over commercially available lateral-flow immunochromatography-based SARS-CoV-2 antigen tests through easily obtainable nasopharyngeal sampling.

Similarly, Raziq *et al.* report a MIP-based electrochemical sensor for the rapid detection of the SARS-CoV-2 nucleocapsid protein (ncovNP). This device is comprised of a disposable sensor chip in the form of a gold thin-film electrode (Au-TFE) interfaced with a MIP selective for ncovNP connected to a portable potentiostat, measuring the reduction in charge transfer intensity carried by the hexacyanoferrate redox probe *via* the thin ncovNP-MIP film to the Au-TFE.[250] Fabrication of the sensor consisted of modifying an Au-TFE with a ncovNP-MIP film *via* electrochemical surface imprinting, utilising poly-m-phenylenediamine as functional monomer – rationalised through computational modelling.[251] The performance of the resulting ncovNP sensor was initially assessed in lysis buffer, signifying a linear response up to 111 fM with an LoD of 15 fM. The rebinding time of ncovNP at the sensor's surface was also optimised to 15 min incubation in ncovNP-containing

samples, as demonstrated by sensor saturation and response equilibrium.[250]

Sensor selectivity was assessed by evaluating its ability to distinguish between ncovNP and interfering proteins such as a subunit of SARS-Cov-2 spike protein, S1 (75 kDa, pI 6.0); hepatitis C virus surface viral antigen, E2 HCV (47 kDa, pI 8.2); Cluster of Differentiation 48 protein, CD48 (22 kDa, pI 9.3); and bovine serum albumin, BSA (66 kDa, pI 4.7). Target protein selection was established by protein size, isoelectric point molecular weight, and potential to be found in real biological samples. Nevertheless, the results highlighted that the response of the ncovNP sensor was greater towards the target protein as compared to the responses towards the interfering proteins.[255]

The clinical diagnostic feasibility of the ncovNP sensor was studied by analysing the nasopharyngeal swab specimens of four COVID-19 negative and four COVID-19 positive patients. The presence or absence of the viral infection in the clinical samples was confirmed with RT-PCR method. Initially, the sensor was calibrated using COVID-19 negative samples spiked with known concentrations of ncovNP. The sensor showed a pseudo-linear response *versus* ncovNP concentration in the range of 0.22–333 fM with a LoD of 27 fM. In addition, the sensor demonstrated appreciable selectivity towards ncovNP, since its response was almost insensitive to the addition of S1 in the COVID-19 negative sample but raised immediately after ncovNP was spiked. These results indicate the sensor's promising capability to respond towards ncovNP without significant disturbance towards the accurate determination of COVID-19 positive samples, where other proteins of SARS-CoV-2 are presented.[250] Finally, sensor stability was inspected *via* the preparation of 12 sensors, which were tested on a weekly basis in the lysis buffer diluted COVID-19 negative samples spiked with ncovNP at a concentration of 66.6 fM. The results confirmed that the response of the as-prepared sensors remained unchanged for up to 9 weeks of storage, revealing excellent long-term stability.[250] The presented strategy presents a new route for the development of express COVID-19 diagnostic tools, relying on an entirely different approach as compared to the currently available SARS-CoV-2 antigen tests. Thus, this method could symbolise a valuable alternative to a portable diagnostic platform for the rapid screening of COVID-19.[250]

Tears

Takeuchi *et al.* successfully demonstrated the use of tears as a physiological database for target biomarkers, enabling the predictive determination of cancer aggression at the onset. The developed molecular imprinting-based dynamic moulding approach, produced antibody-conjugated signalling nanocavities capable of cancer-related small extracellular vesicle (sEVs) recognition.[252] The current *status quo* of *in vivo* sEV detection relies upon the collection of blood samples, micro-ribonucleic acids, and proteins embedded inside and/or outside sEVs.[253] The analysis proceeds *via* RT-PCR, ELISA, Western blotting, and mass spectroscopy.[254] These analytical methods usually involve

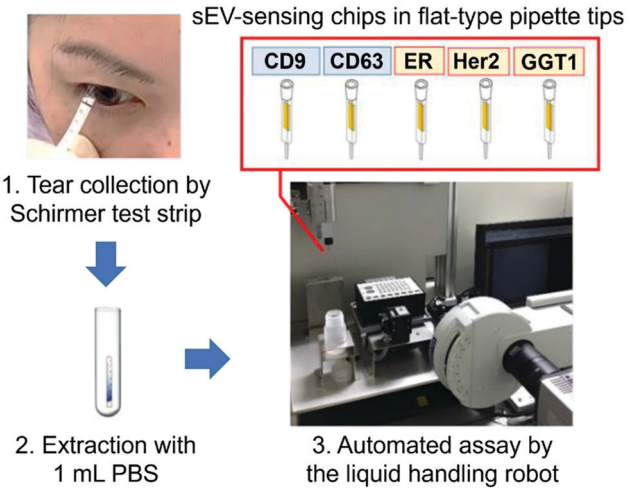

Fig. 13 Detection of breast cancer-related small extracellular vesicles (sEV) available in tear samples using the Schirmer tear test strip. Reproduced with permission from ref. 252, Copyright 2020 ACS Publications.

time-consuming and tedious pre-treatments, such as ultracentrifugation and/or size-exclusion chromatography.[252]

However, tears have been reported to contain sEVs and can be collected easily in a non-invasive manner using the Schirmer tear test strip by placing a filter paper inside the lower lid of the eye for tear extraction (Fig. 13).[255,256] Tears provide a means of convenient and self-collecting sampling at the point-of-care. Thus, Takeuchi *et al.* fabricated a non-invasive, rapid, and sensitive platform for sensing intact sEVs within the tears sampled from breast cancer patients. The synthesis of sEV-binding nanocavities began with the conjugation of silica nanoparticles to hexahistidine peptide chains and free thiol groups as dynamic moulds. Thiol groups were then coupled with methacrylic acid (functional monomer) *via* disulphide exchange reaction with 2-(2-pyridyl)dithioethyl methacrylamide to yield methacrylamide-coupled hexahistidine-tagged silica nanoparticles, enabling copolymerisation with the polymer matrix.[252] Subsequently, surface-initiated atom transfer radical polymerisation was performed to form a layer of 2-methacryloyloxyethyl phosphorylcholine-based biocompatible polymer matrix, whereby the formed coating was intended to minimise non-specific binding to the substrate.[257]

Tears collected from five breast cancer patients and five healthy volunteers were used to assess the efficiency of the sEV sensor chip towards cancer detection. Extracted tear sEVs were analysed exclusive of any pre-treatment, ensuring that those analysed were intact. The LoD was calculated at 1.2×10^{-17} M (linear range of 0–1.0×10^{-16} M), highlighting the comparability of the device in question to previously reported pre-treatment-free methods.[258–263] The authors attributed the sensor's success to the highly dense sEV-sensing nanocavities, antibody orientation, and preferable round shape for small extracellular vesicle binding, enabling small extracellular vesicles to form multipoint interactions with two or more antibodies (anti-CD9).[252]

The developed sensor exhibited selectivity when successfully differentiating between healthy donors and breast cancer patients, as well as between samples collected before and after total mastectomy. Their nano-processing strategy can be easily repurposed for the specific detection of other types of cancer by changing the conjugated antibodies, thereby facilitating the establishment of liquid biopsy for early cancer diagnosis. Sensor development was further enhanced *via* the construction of a differential antibody array for breast cancer-related sEV detection. This involved the conjugation of five antibodies: anti-CD9, anti-CD63, anti-oestrogen receptor, antihuman epidermal growth factor receptor 2, and anti-GGT1 on each small extracellular vesicle-sensing chip. Moreover, the sensor showed an analysis time of 5 min, significantly less than that of ELISA-based strategies.[257]

Here we have explored the use of molecular imprinting technologies as the sensor components in diagnostic tools for the detection of analytes in a wide range of biofluids for the detection of a variety of biomarkers utilised to diagnose disease. The inherent and versatile ability of MIPs to identify pathological biomarkers, ranging from small molecules to whole-cell organisms and viruses was further explored through their ability to detect disease-specific biomarkers in biofluids such as serum, saliva, cerebrospinal fluid, sweat, urine, nasopharyngeal fluid, and tears, signifying MIPs' potential role in the future of precision diagnostics. Recent progress in the field of MIP-biosensing exemplifies their clinically relevant sensitivity and specificity that can be attained by integrating molecular imprinted species with well-established nanomaterials and ''intelligent'' interfaces capable of manipulating and extracting analytes of interest from complex biological media. These cost-effective, highly stable, long shelf-life, artificial sensing elements can provide new avenues for developing non-invasive biosensing platforms for the rapid, accurate, and quantifiable detection of health-relevant biomarkers at point-of-care. A highlighted selection of the MIP-based biosensors targeting biofluid-specific biomarkers and their corresponding detectable diseases discussed in this review, is summarised in Table 4.

Progress towards commercialising MIP-based biosensors

The Freestyle Libre 2, Accutrend® Plus system, and CoaguChek® Pro II (Table 1), are current benchmark examples of commercially available devices where biological materials have been employed as recognition elements for exclusive analyte detection. Throughout this review, from Diouf *et al.* MIP sensor for glucose detection, to Zhang *et al.* development of a wearable MIP sensor for the non-invasive monitoring of lactate in human sweat, the capability and potential of MITs to be replacements of their biological equivalents for the development of personalised medical care has been demonstrated. To date, along with the substantial advancements in developing MIP composites capable of detecting biomarkers in a wide range of biofluids, the field has seen some initial steps towards translating MIP technologies into commercially available products. One non-randomised clinical investigation for a MIP-based medical device aimed to quantifiably monitoring the effect of chemotherapy in colorectal cancer patients *via* the detection of transfer ribonucleic acid markers has been conducted in urine samples. The MIP-based sensor platform was designed to detect adenosine monophosphate by measuring surface acoustic waves in a microfluidic channel.[290] Commercially, among the companies that have emerged, MIP Technologies, based in Lund, Sweden, is an ISO 9001:2008 certified company specialising in the design and production of custom-made polymeric separation materials through two commercialised products; Resna® (bulk resins) and Affinilute™ MIP Columns (solid-phase extraction columns) for separation.[291] Allergy Amulet has marketed a point-of-care device to detect allergens at ''clinically relevant thresholds'' *via* MIP electrochemical sensing. The MIP detection element of the device was based on the electrochemical oxidation *via* differential pulse voltammetry of o-phenylenediamine (functional monomer) onto screen-printed electrodes under nitrogen atmosphere.[292,293] MIP Diagnostics, based in Bedford, U.K., has been exploring the commercialisation of MIT through their ''nanoMIPs'' platform promoted for its use in the development of lateral flow devices and ELISA assays. Nanoparticle MIPs and nanoMIPs, are produced *via* bulk polymerisation using styrene as functional monomer, ethylene glycol dimethacrylate and trimethylolpropane trimethacrylate as crosslinkers, *N*-diethyldithiocarbamic acid benzyl ester as interferer, and pentaerythritol-tetrakis-(3-mercaptopropionate) as chain transfer agent, dissolved in acetonitrile using glass beads and UV polymerised. Depending on the application, the nanoMIPs have been subsequently conjugated onto sensor chips *via* coupling using carbodiimide crosslinker chemistry or through activation of the nanoMIP particles using NaOH, silanisation of the sensor chip's surface and subsequent immobilisation, among others.[294–297] Their current research and development products (Troponin I, ProBNP and NT-ProBNP) rely on the nanoMIPs as the affinity reagent. As the biosensors market is anticipated to exceed $35 billion by 2026, following an increased demand for point-of-care healthcare monitoring and wearables, we foresee subsequent expansion to the commercialisation interest of MIT, allowing for growth opportunities in the research and development of smart MIP-based biodevices with a drive-in sustainable synthesis approaches.[298]

Summary and future outlook

The function of MIPs performing as the synthetic recognition components within biosensors is motivated by improving healthcare technologies. However, to commercially compete with their biological counterparts further developments are required to accelerate the performance of MIP sensors in the application of clinical samples. Although the expansion of MIP-based point-of-care devices or other wearable sensors could still benefit from further development, the direct results obtained from using these simple biomarker detection techniques provide an accurate, rapid, convenient, reliable, affordable, and sustainable approach for on-site disease diagnostics.

Table 4 Summary and additional MIP-based biosensors in the literature for the detection of biological analytes in a variety of different physiological media

Biological analyte	Biological media	Disease detection	Sensor	Linear ranges	Limit of detection	Ref.
Amyloid-β	Serum	Alzheimer's disease	Voltammetric	5 pg mL^{-1}–10 ng mL^{-1}	1.22 pg mL^{-1}	166
D-/L-Aspartic acid	CSF	Neurological	Voltammetric	1.73–1.79 ng mL^{-1}	1.79 ng mL^{-1}	136
Bilirubin	Saliva	Liver function	Voltammetric and impedimetric	12.08–91.81 fM	7.8 fM	200
Carcinoembryonic antigen	Serum	Cancer	Fluorometric	0.01–100 ng mL^{-1}	3.0 pg mL^{-1} (green) 1.3 pg mL^{-1} (yellow)	264
Cholecystokinin neuropeptides	CSF	Central nervous system	MALDI-ToF MS	0.02–2.0 μg mL^{-1}	1.2 and 5.5 pM	212
Cortisol	Saliva	Cardiovascular disease	Colorimetric	2.50–20.0 ng mL^{-1}	1.02 ng mL^{-1}	193
Cortisol	Saliva	Cardiovascular disease	Impedimetric	0.50–64.0 nM	0.14 nM	265
Cortisol	Sweat	Cardiovascular disease	OECTs	0.10–1.0 μM	2.68 μA dec^{-1}	135
Cortisol	Saliva	Stress	LMR	0–1.0 × 10^{-6} g mL^{-1}	2.59 × 10^{-14} g mL^{-1}	266
Cortisol	Sweat	Stress	Capacitive	10–66 ng mL^{-1}	2.0 ng mL^{-1} (±0.4)	218
Cortisol	Artificial sweat	Stress	Amperometric	10 × 10^{-9}–1 × 10^{-6} M	0.2 × 10^{-9} M	225
Cholesterol	Serum	Coronary heart disease	Voltammetric	1.0 × 10^{-18}–10^{-13} M	3.30 × 10^{-19} M	165
Cytochrome *C*	Urine	Apoptosis	Fluorometric	0.20–60.0 μM	0.11 μM	267
L-Dopa	Serum	Parkinson's disease	Electrochemical	0.40–100 μM	1.20 × 10^{-2} μM	268
Dopamine	Artificial CSF	Schizophrenia	Voltammetric	0.30–100 μM	0.10 μM	209
Dopamine	Urine	Parkinson's disease	Optical	8.0–200.0 ng mL^{-1}	1.50 ng mL^{-1}	269
Estriol	Serum	Breast cancer	Amperometric	0.10–20.0 μg mL^{-1}	2.0 × 10^{-3} μg mL^{-1}	163
Ferritin	Plasma	Kidney damage	Voltammetric	120.0–360.0 mg dm^{-3}	10.7 mg dm^{-3}	229
α-Fetoprotein	Serum	Cancer	Fluorometric	0.01–100 ng mL^{-1}	5.0 pg mL^{-1} (green) 2.2 pg mL^{-1} (yellow)	264
α-Fetoprotein	Saliva	Cancer	Fluorometric	0.01–100 ng mL^{-1}	5.1 pg mL^{-1} (green) 1.1 pg mL^{-1} (yellow)	264
Galectin-3	Serum	Heart failure	SPR	10.0–50.0 ng mL^{-1}	2.0 ng mL^{-1}	270
Glucose	Saliva	Diabetes	Voltammetric and imedimetric	0.5–50 μg mL^{-1}	0.59 μg mL^{-1} and 1.6 μg mL^{-1}	196
Glucose	Saliva	Diabetes	Potentiometric	3.20 × 10^{-7}–1.0 × 10^{-3} M	1.9 × 10^{-7} M (± 0.15)	137
Glucose	Synthetic tears	Diabetes	Fluorometric	3.0–16.0 mM	10.0 μg mL^{-1}	271
Haemoglobin	Urine	Anaemia	Potentiometric	1.0–10.0 μg mL^{-1}	1.0 μg mL^{-1}	138
HIV	Serum	HIV	Electrochemiluminescence	0.30–3.0 nM	3.0 × 10^{-7} nM	164
HIV-p24	Serum	HIV-p24	Voltammetric	1.0 × 10^{-4}–2 ng cm^{-3}	8.3 × 10^{-5} ng cm^{-3}	162
HAS	Serum	Coronary heart disease	QCM	5.0 × 10^{-5}– × 10^{-4} g L^{-1}	2.60 × 10^{-5} g L^{-1}	236
HAS	Serum	Coronary heart disease	Voltammetric	8.0 × 10^{-4}–2.0 × 10^{-2} g L^{-1}	1.60 × 10^{-5} g L^{-1}	234
HAS	Serum	Coronary heart disease	Fluorometric	1.70 × 10^{-2}–3.0 × 10^{-1} g L^{-1}	2.90 × 10^{-3} g L^{-1}	233
HAS	Serum	Coronary heart disease	Voltammetric	1.99 × 10^{-6}–30.91 × 10^{-6} g L^{-1}	4.20 × 10^{-6} g L^{-1}	210
HAS	Plasma	Coronary heart disease	Voltammetric	1.0 × 10^{-10}–10^{-4} g L^{-1}	2.0 × 10^{-11} g L^{-1}	235
HAS	Urine	Diabetes	Voltammetric	1.0 × 10^{-10}–10^{-4} g L^{-1}	3.0 × 10^{-11} g L^{-1}	231
HAS	Urine	Kidney damage	Voltammetric	0.02–0.10 g L^{-1}	3.70 g L^{-1}	229
Insulin	Serum	Diabetes	MALDI-ToF MS	23.6 ± 2.27 μM	0.5 ng mL^{-1}	134
Interleukin-8	Saliva	Oral cancer	Voltammetric	0.10–10.0 pM	4.0 × 10^{-2} pM	194
Japanese encephalitis virus	Serum	Japanese encephalitis virus	Resonance light scattering	0–25 pM	1.3 pM	272
Lactate	Sweat	Anerobic metabolism	Voltammetric	1.0 × 10^{-6}–10^{-1} M	0.22 μM	226
Lactate	Sweat	Cell acidosis	Voltammetric	1.0 × 10^{-6}–10^{-1} M	2.20 × 10^{-7} M	226
Lysozyme	Synthetic saliva	Chronic disease	Impedimetric	2.20–292 mg L^{-1}	0.9 mg L^{-1} and 2.1 mg L^{-1}	273
Lysozyme	Saliva and urine	Chronic disease	Fluorometric	1.0 × 10^{-7}–×10^{-6} M	1.02 × 10^{-8} M	274
Melatonin	Urine	Urinary tract infection	Voltammetric	1.75–2.11 pg mL^{-1}	20.0 pg mL^{-1}	230
Melatonin	Plasma and urine	Parkinson's disease	Amperometry	5.20 × 10^{-2}–100 μm L^{-1}	6.0 × 10^{-9} μM	275
Myoglobin	Serum	Myocardial infarction	Spectrophotometrically	0.50–3.50 mg mL^{-1}	623.0 mg g^{-1}	276
Norepinephrine	Urine	Bronchial asthma	Electrochemical	0.50–80.0 μM	0.10 μM	277
3-Nitrotyrosine	Serum and urine	Alzheimer's disease	Electrochemical	0.20–50.0 μM	0.05 μM	278
3-Nitrotyrosine	Serum	Atherosclerosis	Fluorometric	5.0 × 10^{-2}–1.85 μM	1.70 × 10^{-2} μM	279
3-Nitrotyrosine	Urine	Neurodegenerative disorders	HPLC with SPE	2.50–55.0 μg mL^{-1}	0.70 μg mL^{-1}	280
3-Nitrotyrosine	Serum	Neurodegenerative disorders	SPR	0.50–1.0 × 10^{3} pM	0.135 pM	281
3-Nitrotyrosine	Urine	Oxidative stress	Voltammetric	10 pg mL^{-1}–1 μg mL^{-1}	1.13 pg mL^{-1}	237

Table 4 (*continued*)

Biological analyte	Biological media	Disease detection	Sensor	Linear ranges	Limit of detection	Ref.
ncovNP	Nasopharyngeal fluid	COVID-19	Electrochemical	0.22–333 fM	27 fM	250
ncovS1	Nasopharyngeal fluid	COVID-19	Electrochemical	0–30 pg mL^{-1}	4.8 pg mL^{-1}	245
Oxidised glutathione	Plasma	Cardiovascular disease	Amperometric	0–86 × 10^{-7} M	1.86 × 10^{-9} M	282
Phycocyanin	Urine	Cyanobacterial blooms	Fluorometric	7.5 × 10^{-2} μM	0.80–8.0 μM	283
D-/L-Pyroglutamic acid	Urine	Infection	Voltammetric	1.80–173.6 ng mL^{-1}	5.43 × 10^{3}–5.24 × 10^{5} ng mL^{-1}	211
	CSF			1.50–180 ng mL^{-1}	2.52 × 10^{3}–3.03 × 10^{5} ng mL^{-1}	
	Plasma			1.30–153.8 ng mL^{-1}	1.08 × 10^{3}–1.28 × 10^{5} ng mL^{-1}	
Sarcosine	Urine	Cancer	RIS	0.25–3.0 mM	4.50 × 10^{-5} nM	284
D-/L-Serine	Serum	Schizophrenia	Voltammetric	0.83–20.63 ng mL^{-1} (D-)	0.24 ng mL^{-1} (D-)	168
				0.87–20–45 ng mL^{-1} (L-)	0.25 ng mL^{-1} (L-)	
Tryptamine	CSF	Cardiovascular disease	Fluorometric	0.3–1.5μmol L^{-1}	1.46 μmol L^{-1}	285
Tryptophan	Serum	Schizophrenia	Voltammetric	0.01–4.0 μM	8.0 × 10^{-13} μM	286
				4.0–20.0 μM		
				20.0–100.0 μM		
Tyrosine	Serum	Parkinson's disease	Voltammetric	0.1–400.0 μM	4.60 × 10^{-2} μM	287
Uric acid	Urine	Hyperuricemia	SPR	0.50–40.0 mg L^{-1}	0.25 mg L^{-1}	288
Uric acid	Urine	Hyperpiesia	Voltammetric	0.1–100.0 μM	3.20 × 10^{-3} μM	287
Zika virus	Saliva	Zika virus	Potentiometric	2.4 × 10^{-1}–5.3 × 10^{6} PFU	10.0 PFU mL^{-1}	289

Cerebrospinal fluid (CSF), matrix-assisted laser desorption/ionisation-time of flight mass spectroscopy (MALDI-ToF MS), organic electrochemical transistors (OECTs), lossy mode resonance (LMR), surface plasmon resonance (SPR), human immunodeficiency virus (HIV), human serum albumin (HSA), quartz crystal microbalance (QCM), solid-phase extraction (SPE), field-effect transistor (FET), and reflectometric interferometric spectroscopy (RIS).

MIP biosensors' high selectivity and sensitivity, miniaturised into portable devices, will inspire universally affordable and reliable biofluid detection.

The synthetic affinity acquired through the "molecular memory" of the imprinted cavities towards a target species has signified the importance of molecular imprinting approaches, concerning the ability of such recognition matrices to identify specific analytes in complex mediums and their subsequent importance in diagnostics. This review has further demonstrated the ability of MIPs acting as sensing elements to present the required stability akin to selectivity and performance to that of enzymatic and antibody-based diagnostic counterparts *via* summarising the current status of the most up-to-date molecularly imprinted biosensor devices. The rudiments of MIP design, including the fundamental elements (*e.g.*, functional monomer(s), crosslinker, initiator *etc.*), preparative methods, and characterisation techniques, have been evaluated, highlighting innovative and/or improved processes, such as bulk, emulsion, suspension, precipitation, and electropolymerisation, in addition to, sol–gel, surface, and epitope imprinting processes.

Integrating MIPs with nanocomposites to detect and purify biomarkers out of small volumes of biofluids has been critical for developing sensing platforms. As can be seen by the literature covered, incorporating smart technologies, and miniaturising the sensing element of such devices are important aspects of future commercialisation.

From small molecules to the advancement of facile methodologies, such as electropolymerisation, capable of imprinting macromolecules, whole microorganisms, and viruses, molecular imprinting has effectively expanded its ability to extend toward the detection of a wide range of biomarkers.

Until now, MIPs for biosensing has predominately focused on imprinting single species followed by optimisation, selectivity assessment in the presence of structurally homologous species and improved performance. Nonetheless, early disease detection predominately relies on the simultaneous identification of several biomarkers coexistent in the same media. The design and expansion of strategies towards the development of multiplexed sensing platforms or arrays of disease-relevant biomarkers can further expand the clinical significance of MIP-biosensors.

While lab-scale molecular imprinting has significantly progressed and there are many positive indicators of its future role in medical diagnostics, sustainable approaches to their production by employing green chemistry principles, is an essential element that needs to be addressed. As the principles of green chemistry are becoming more relevant to several scientific fields, molecular imprinting is destined to follow. At present, there has been disproportionate and insufficient research focusing on the use of less toxic and green chemicals that are less harmful to the users and non-polluting to the environment. Through green synthesis, the selection of green and renewable sourced reagents, reducing the number of reagents required for the processes, and the engagement of safer analytical methods, strategies focusing on sustainability and a "toxic-free"

environment can be attained, contributing to both healthcare and environmental sustainability.

Conflicts of interest

The authors have no conflicts of interest to declare.

Acknowledgements

The authors gratefully acknowledge financial support from the Engineering and Physical Sciences Research Council Grant EP/V010859/1 and the Royal Society Research Grant RSG\R1\201185. Fig. 1 and 2 and ToC were created with BioRender.com.

References

1 J. L. J. M. Müskens, R. B. Kool, S. A. van Dulmen and G. P. Westert, *BMJ Qual. Saf.*, 2022, **31**, 54–63.
2 M.-S. Ong, F. Magrabi and E. Coiera, *BMC Health Serv. Res.*, 2018, **18**, 1–8.
3 I. M. Lubin, J. R. Astles, S. Shahangian, B. Madison, R. Parry, R. L. Schmidt and M. L. Rubinstein, *Diagnosis*, 2021, **8**, 281–294.
4 J. Tu, R. M. Torrente-Rodríguez, M. Wang and W. Gao, *Adv. Funct. Mater.*, 2020, **30**, 1906713.
5 T. Pinheiro, A. R. Cardoso, C. E. A. Sousa, A. C. Marques, A. P. M. Tavares, A. M. Matos, M. T. Cruz, F. T. C. Moreira, R. Martins and E. Fortunato, *ACS Omega*, 2021, **6**, 29268–29290.
6 S. A. Abid, A. A. Muneer, I. M. S. Al-Kadmy, A. A. Sattar, A. M. Beshbishy, G. E.-S. Batiha and H. F. Hetta, *Life Sci.*, 2021, **273**, 119117.
7 R. Samson, G. R. Navale and M. S. Dharne, *3 Biotech.*, 2020, **10**, 1–9.
8 A. Parihar, P. Ranjan, S. K. Sanghi, A. K. Srivastava and R. Khan, *ACS Appl. Bio Mater.*, 2020, **3**, 7326–7343.
9 L. Xu, D. Li, S. Ramadan, Y. Li and N. Klein, *Biosens. Bioelectron.*, 2020, **170**, 112673.
10 **https://www.freestylelibre.co.uk**, FreeStyle Libre.
11 **https://diagnostics.roche.com/global/en/products/instruments/accutrend-plus**, Accutrend® Plus System.
12 **https://diagnostics.roche.com/gb/en/products/instruments/coaguchek-pro-ii**, CoaguChek® Pro II.
13 C.-C. Hong, C.-P. Chen, J.-C. Horng and S.-Y. Chen, *Biosens. Bioelectron.*, 2013, **50**, 425–430.
14 C. Lorenz, F. von Pelchrzim and R. Schroeder, *Nat. Protoc.*, 2006, **1**, 2204–2212.
15 L. Pauling, *J. Am. Chem. Soc.*, 1940, **62**, 2643–2657.
16 M. V. Polyakov, *Zh. Fiz. Khim.*, 1931, **2**, 799–805.
17 F. Canfarotta, A. Poma, A. Guerreiro and S. Piletsky, *Nat. Protoc.*, 2016, **11**, 443–455.
18 L. Ye, Y. Yu and K. Mosbach, *Analyst*, 2001, **126**, 760–765.
19 J. Pan, W. Chen, Y. Ma and G. Pan, *Chem. Soc. Rev.*, 2018, **47**, 5574–5587.
20 G. Vasapollo, R. Del Sole, L. Mergola, M. R. Lazzoi, A. Scardino, S. Scorrano and G. Mele, *Int. J. Mol. Sci.*, 2011, **12**, 5908–5945.
21 E. V. Piletska, A. R. Guerreiro, M. J. Whitcombe and S. A. Piletsky, *Macromolecules*, 2009, **42**, 4921–4928.
22 A. Poma, A. P. F. Turner and S. A. Piletsky, *Trends Biotechnol.*, 2010, **28**, 629–637.
23 G. Wulff, *Angew. Chem., Int. Ed. Engl.*, 1995, **34**, 1812–1832.
24 S. Yan, Y. Fang and Z. Gao, *Biosens. Bioelectron.*, 2007, **22**, 1087–1091.
25 C. Alexander, H. S. Andersson, L. I. Andersson, R. J. Ansell, N. Kirsch, I. A. Nicholls, J. O'Mahony and M. J. Whitcombe, *J. Mol. Recognit.*, 2006, **19**, 106–180.
26 E. Reville, E. Sylvester, S. Benware, S. Negi and E. B. Berda, *Polym. Chem.*, 2022, **13**, 3387–3411.
27 L. Ye and K. Mosbach, *Chem. Mater.*, 2008, **20**, 859–868.
28 Z. El-Schich, Y. Zhang, M. Feith, S. Beyer, L. Sternbæk, L. Ohlsson, M. Stollenwerk and A. G. Wingren, *Biotechniques*, 2020, **69**, 406–419.
29 D. Refaat, M. G. Aggour, A. A. Farghali, R. Mahajan, J. G. Wiklander, I. A. Nicholls and S. A. Piletsky, *Int. J. Mol. Sci.*, 2019, **20**, 6304.
30 M. Komiyama, T. Mori and K. Ariga, *Bull. Chem. Soc. Jpn.*, 2018, **91**, 1075–1111.
31 Y. Taguchi, E. Takano and T. Takeuchi, *Langmuir*, 2012, **28**, 7083–7088.
32 K. Yoshimatsu, K. Reimhult, A. Krozer, K. Mosbach, K. Sode and L. Ye, *Anal. Chim. Acta*, 2007, **584**, 112–121.
33 Y. Ge and A. P. F. Turner, *Eur. J. Chem.*, 2009, **15**, 8100–8107.
34 J. Haginaka, K. Nishimura, T. Kimachi, K. Inamoto, Y. Takemoto and Y. Kobayashi, *Talanta*, 2019, **205**, 120149.
35 J. J. BelBruno, *Chem. Rev.*, 2018, **119**, 94–119.
36 J. Xu, H. Miao and L. Zou, *Angew. Chem., Int. Ed.*, 2021, **60**, 24526–24533.
37 E. N. Ndunda, *J. Mol. Recognit.*, 2020, **33**, e2855.
38 B. Sellergren, *Molecularly imprinted polymers: man-made mimics of antibodies and their application in analytical chemistry*, Elsevier, 2000.
39 B. Mattiasson and L. Ye, *Molecularly imprinted polymers in biotechnology*, Springer, 2015, vol. 150.
40 L. Ye and K. Mosbach, *React. Funct. Polym.*, 2001, **48**, 149–157.
41 K. Haupt, P. X. Medina Rangel and B. T. S. Bui, *Chem. Rev.*, 2020, **120**, 9554–9582.
42 R. Arshady and K. Mosbach, *Die Makromol. Chem.*, 2003, **182**, 687–692.
43 T. Takeuchi and J. Matsui, *Acta Polym.*, 1996, **47**, 471–480.
44 G. Wulff, A. Sarhan and K. Zabrocki, *Tetrahedron Lett.*, 1973, **14**, 4329–4332.
45 K. Mosbach and O. Ramström, *Bio/Technology*, 1996, **14**, 163–170.
46 J. O'Mahony, A. Molinelli, K. Nolan, M. R. Smyth and B. Mizaikoff, *Biosens. Bioelectron.*, 2006, **21**, 1383–1392.
47 S. N. N. S. Hashim, R. I. Boysen, L. J. Schwarz, B. Danylec and M. T. W. Hearn, *J. Chromatogr. A*, 2014, **1359**, 35–43.

48 **https://www.niehs.nih.gov/health/topics/science/biomarkers/index.cfm**, National Institute of Environmental Health Sciences.
49 S. Emaminejad, W. Gao, E. Wu, Z. A. Davies, H. Y. Y. Nyein, S. Challa, S. P. Ryan, H. M. Fahad, K. Chen and Z. Shahpar, *Proc. Natl. Acad. Sci. U. S. A.*, 2017, **114**, 4625–4630.
50 W. Gao, H. Y. Y. Nyein, Z. Shahpar, H. M. Fahad, K. Chen, S. Emaminejad, Y. Gao, L.-C. Tai, H. Ota and E. Wu, *ACS Sens.*, 2016, **1**, 866–874.
51 J. Heikenfeld, A. Jajack, B. Feldman, S. W. Granger, S. Gaitonde, G. Begtrup and B. A. Katchman, *Nat. Biotechnol.*, 2019, **37**, 407–419.
52 A. Martin-Esteban, *Fresenius' J. Anal. Chem.*, 2001, **370**, 795–802.
53 W.-C. Lee, C.-H. Cheng, H.-H. Pan, T.-H. Chung and C.-C. Hwang, *Anal. Bioanal. Chem.*, 2008, **390**, 1101–1109.
54 G. Liu, Y. She, S. Hong, J. Wang and D. Xu, *Appl. Sci.*, 2018, **8**, 560.
55 R. J. Ansell, J. K. L. Kuah, D. Wang, C. E. Jackson, K. D. Bartle and A. A. Clifford, *J. Chromatogr. A*, 2012, **1264**, 117–123.
56 L. Chen, X. Wang, W. Lu, X. Wu and J. Li, *Chem. Soc. Rev.*, 2016, **45**, 2137–2211.
57 L. M. Madikizela, S. S. Zunngu, N. Y. Mlunguza, N. T. Tavengwa, P. S. Mdluli and L. Chimuka, *Water SA*, 2018, **44**, 406–418.
58 Y. Yang, Q. Li, G. Fang and S. Wang, *RSC Adv.*, 2016, **6**, 54510–54517.
59 N. Sohrabi, R. Mohammadi, H. R. Ghassemzadeh and S. S. S. Heris, *Microchem. J.*, 2022, **175**, 107087.
60 Y. A. Olcer, M. Demirkurt, M. M. Demir and A. E. Eroglu, *RSC Adv.*, 2017, **7**, 31441–31447.
61 R. Pratiwi, S. Megantara, D. Rahayu, I. Pitaloka and A. N. Hasanah, *J. Young Pharm.*, 2019, **11**, 12.
62 S. Pardeshi and S. K. Singh, *RSC Adv.*, 2016, **6**, 23525–23536.
63 W. Siripairoj, A. Kaewchada and A. Jaree, *J. Taiwan Inst. Chem. Eng.*, 2014, **45**, 338–346.
64 K. Ji, X. Luo, L. He, S. Liao, L. Hu, J. Han, C. Chen, Y. Liu and N. Tan, *J. Pharm. Biomed. Anal.*, 2020, **180**, 113036.
65 V. B. Kandimalla and H. Ju, *Anal. Bioanal. Chem.*, 2004, **380**, 587–605.
66 E. Daniels, Y. L. Mustafa, C. Herdes and H. S. Leese, *ACS Appl. Bio Mater.*, 2021, **4**, 7243–7253.
67 M. Yoshikawa, K. Tharpa and S.-O. Dima, *Chem. Rev.*, 2016, **116**, 11500–11528.
68 X. Shen, C. Xu and L. Ye, *Soft Matter*, 2012, **8**, 7169–7176.
69 C. Gomes, G. Sadoyan, R. Dias and M. R. P. F. N. Costa, *Processes*, 2017, **5**, 72.
70 J. Peng, D. Xiao, H. He, H. Zhao, C. Wang, T. Shi and K. Shi, *J. Sep. Sci.*, 2016, **39**, 383–390.
71 M. Díaz-Álvarez, E. Turiel and A. Martín-Esteban, *J. Chromatogr. A*, 2016, **1469**, 1–7.
72 A. Beltran, R. M. Marcé, P. A. G. Cormack and F. Borrull, *J. Chromatogr. A*, 2009, **1216**, 2248–2253.
73 Y. Liu, K. Hoshina and J. Haginaka, *Talanta*, 2010, **80**, 1713–1718.
74 T. Alizadeh, *Anal. Chim. Acta*, 2010, **669**, 94–101.
75 K. H. J. Buschow, M. C. Flemings and R. Cahn, *The Encyclopedia of Materials: Science and Technology*, Pergamon Imprint, 2001.
76 G. Zhao, J. Liu, M. Liu, X. Han, Y. Peng, X. Tian, J. Liu and S. Zhang, *Appl. Sci.*, 2020, **10**, 2868.
77 X. Ma, Z. Meng, L. Qiu, J. Chen, Y. Guo, D. Yi, T. Ji, H. Jia and M. Xue, *J. Chromatogr. B: Anal. Technol. Biomed. Life Sci.*, 2016, **1020**, 1–5.
78 E. Vivaldo-Lima, P. E. Wood, A. E. Hamielec and A. Penlidis, *Ind. Eng. Chem. Res.*, 1997, **36**, 939–965.
79 R. R. Watson, *Polyphenols in plants: isolation, purification and extract preparation*, Academic Press, 2018.
80 C. Gomes, G. Sadoyan, R. Dias and M. R. P. F. N. Costa, *Processes*, 2017, **5**, 72.
81 L. J. Schwarz, M. K. Potdar, B. Danylec, R. I. Boysen and M. T. W. Hearn, *Anal. Methods*, 2015, **7**, 150–154.
82 H. Cao, J. B. Xiao and M. Xu, *Macromol. Res.*, 2006, **14**, 324–330.
83 S. Ma, X. Zhuang, H. Wang, H. Liu, J. Li and X. Dong, *Anal. Lett.*, 2007, **40**, 321–333.
84 F.-F. Chen, X.-Y. Xie and Y.-P. Shi, *J. Chromatogr. A*, 2013, **1300**, 112–118.
85 Y. Li, H.-H. Yang, Q.-H. You, Z.-X. Zhuang and X.-R. Wang, *Anal. Chem.*, 2006, **78**, 317–320.
86 S. R. Carter and S. Rimmer, *Adv. Funct. Mater.*, 2004, **14**, 553–561.
87 J. Yu, X. Wang, Q. Kang, J. Li, D. Shen and L. Chen, *Environ. Sci.: Nano*, 2017, **4**, 493–502.
88 M. M. Titirici, A. J. Hall and B. Sellergren, *Chem. Mater.*, 2002, **14**, 21–23.
89 R. Wang, L. Wang, J. Yan, D. Luan, J. Wu and X. Bian, *Talanta*, 2021, **226**, 122135.
90 M. Zhang, H. T. Zhao, X. Yang, W. T. Zhang, J. Wang, G. Y. Liu, H. Zhang and A. J. Dong, *RSC Adv.*, 2016, **6**, 3714–3722.
91 F. Ning, T. Qiu, Q. Wang, H. Peng, Y. Li, X. Wu, Z. Zhang, L. Chen and H. Xiong, *Food Chem.*, 2017, **221**, 1797–1804.
92 H. Dai, D. Xiao, H. He, H. Li, D. Yuan and C. Zhang, *Microchim. Acta*, 2015, **182**, 893–908.
93 Y. Wang, J. Zhou, B. Zhang, L. Tian, Z. Ali and Q. Zhang, *Chem. Eng. J.*, 2017, **327**, 932–940.
94 Y. Qu, L. Qin, X. Liu and Y. Yang, *Chemosphere*, 2020, **251**, 126376.
95 J. Cheng, P. R. Chang, P. Zheng and X. Ma, *Ind. Eng. Chem. Res.*, 2014, **53**, 1415–1421.
96 G. Liu, X. Yang, T. Li, Y. She, S. Wang, J. Wang, M. Zhang, F. Jin, M. Jin and H. Shao, *Mater. Lett.*, 2015, **160**, 472–475.
97 X. Wang, G. Chen, P. Zhang and Q. Jia, *Anal. Methods*, 2021, **13**, 1660–1671.
98 R. Xing, Y. Ma, Y. Wang, Y. Wen and Z. Liu, *Chem. Sci.*, 2019, **10**, 1831–1835.
99 A. Rachkov and N. Minoura, *Biochim. Biophys. Acta, Protein Struct. Mol. Enzymol.*, 2001, **1544**, 255–266.
100 A. Rachkov and N. Minoura, *J. Chromatogr. A*, 2000, **889**, 111–118.

101 K. Yang, S. Li, L. Liu, Y. Chen, W. Zhou, J. Pei, Z. Liang and Y. Zhang, *Adv. Mater.*, 2019, **31**, 1902048.
102 A. Tang, L. Duan, M. Liu and X. Dong, *J. Mater. Chem. B*, 2016, **4**, 7464–7471.
103 S. Li, K. Yang, B. Zhao, X. Li, L. Liu, Y. Chen, L. Zhang and Y. Zhang, *J. Mater. Chem. B*, 2016, **4**, 2739.
104 S. Gatto, G. Ball, F. Onida, H. M. Kantarjian, E. H. Estey and M. Beran, *Blood*, 2003, **102**, 1622–1625.
105 E. Yilmaz, O. Ramström, P. Möller, D. Sanchez and K. Mosbach, *J. Mater. Chem.*, 2002, **12**, 1577–1581.
106 K. Kajihara, *J. Asian Ceram. Soc.*, 2013, **1**, 121–133.
107 A. Florea, O. Hosu, B. Ciui and C. Cristea, *Molecularly imprinted polymer-based sensors for biomedical and environmental applications*, Scrievener Publishing, NJ, USA, 2016.
108 C. Guoning, S. Hua, L. Wang, H. Qianqian, C. Xia, Z. Hongge, L. Zhimin, C. Chun and F. Qiang, *J. Pharm. Biomed. Anal.*, 2020, **190**, 113511.
109 R. Rolla, D. Vay, E. Mottaran, M. Parodi, N. Traverso, S. Aricó, M. Sartori, G. Bellomo, L. W. Klassen and G. M. Thiele, *Hepatology*, 2000, **31**, 878–884.
110 S. Sang, Y. Li, X. Guo, B. Zhang, X. Xue, K. Zhuo, C. Zhao, W. Zhang and Z. Yuan, *Biosens. Bioelectron.*, 2019, **141**, 111399.
111 W.-F. Chang, S.-Y. Huang, R.-H. Lee and Y.-C. Liu, *J. Polym. Res.*, 2014, **21**, 1–7.
112 M. C. Blanco-López, M. J. Lobo-Castañón, A. J. Miranda-Ordieres and P. Tunon-Blanco, *TrAC, Trends Anal. Chem.*, 2004, **23**, 36–48.
113 S. A. Piletsky and A. P. F. Turner, *Electroanalysis*, 2002, **14**, 317–323.
114 G. Fomo, T. Waryo, U. Feleni, P. Baker and E. Iwuoha, *Electrochemical Polymerization*, ed. Jafar Mazumder, M. A., Sheardown, H., Al-Ahmed, A., 2019, pp. 105–131.
115 A. Herrera-Chacón, X. Cetó and M. del Valle, *Anal. Bioanal. Chem.*, 2021, **413**, 6117–6140.
116 C. Malitesta, I. Losito and P. G. Zambonin, *Anal. Chem.*, 1999, **71**, 1366–1370.
117 C. Malitesta, F. Palmisano, L. Torsi and P. G. Zambonin, *Anal. Chem.*, 1990, **62**, 2735–2740.
118 R. N. Goyal and S. P. Singh, *Electrochim. Acta*, 2006, **51**, 3008–3012.
119 L. Özcan and Y. Şahin, *Sens. Actuators, B*, 2007, **127**, 362–369.
120 F. Gu, W. He, S. Xiao, S. Wang, X. Li, Q. Zeng, Y. Ni and L. Han, *Sci. Rep.*, 2020, **10**, 1–8.
121 A. Ramanaviciene and A. Ramanavicius, *Biosens. Bioelectron.*, 2004, **20**, 1076–1082.
122 G. Ceolin, Á. Orbán, V. Kocsis, R. E. Gyurcsányi, I. Kézsmárki and V. Horváth, *J. Mater. Sci.*, 2013, **48**, 5209–5218.
123 G. Evtugyn, A. Porfireva, A. Ivanov, O. Konovalova and T. Hianik, *Electroanalysis*, 2009, **21**, 1272–1277.
124 J. Kronholm, K. Hartonen and M.-L. Riekkola, *TrAC, Trends Anal. Chem.*, 2007, **26**, 396–412.
125 G.-Q. Fu, H. Yu and J. Zhu, *Biomaterials*, 2008, **29**, 2138–2142.
126 A. Adumitraăchioaie, M. Tertiș, A. Cernat, R. Săndulescu and C. Cristea, *Int. J. Electrochem. Sci.*, 2018, **13**, 2556–2576.
127 M. Gao, Y. Gao, G. Chen, X. Huang, X. Xu, J. Lv, J. Wang, D. Xu and G. Liu, *Front. Chem.*, 2020, **8**, 1142.
128 P. Jolly, V. Tamboli, R. L. Harniman, P. Estrela, C. J. Allender and J. L. Bowen, *Biosens. Bioelectron.*, 2016, **75**, 188–195.
129 N. Idil and B. Mattiasson, *Sensors*, 2017, **17**, 708.
130 M. Jia, Z. Zhang, J. Li, X. Ma, L. Chen and X. Yang, *TrAC, Trends Anal. Chem.*, 2018, **106**, 190–201.
131 S. A. Zaidi, *Crit. Rev. Anal. Chem.*, 2021, **51**, 609–618.
132 A. Ahmed, J. V. Rushworth, N. A. Hirst and P. A. Millner, *Clin. Microbiol. Rev.*, 2014, **27**, 631–646.
133 O. Lazcka, F. J. del Campo and F. X. Munoz, *Biosens. Bioelectron.*, 2007, **22**, 1205–1217.
134 Z. Wang, X. Fang, N. Sun and C. Deng, *Anal. Chim. Acta*, 2020, **1128**, 1–10.
135 O. Parlak, S. T. Keene, A. Marais, V. F. Curto and A. Salleo, *Sci. Adv.*, 2018, **4**, eaar2904.
136 B. B. Prasad, A. Srivastava and M. P. Tiwari, *Mater. Sci. Eng., C*, 2013, **33**, 4071–4080.
137 D.-M. Kim, J.-M. Moon, W.-C. Lee, J.-H. Yoon, C. S. Choi and Y.-B. Shim, *Biosens. Bioelectron.*, 2017, **91**, 276–283.
138 T. S. Anirudhan and S. Alexander, *Eur. Polym. J.*, 2017, **97**, 84–93.
139 D. Ivnitski, I. Abdel-Hamid, P. Atanasov and E. Wilkins, *Biosens. Bioelectron.*, 1999, **14**, 599–624.
140 X. Shen, J. Svensson Bonde, T. Kamra, L. Bülow, J. C. Leo, D. Linke and L. Ye, *Angew. Chem., Int. Ed.*, 2014, **53**, 10687–10690.
141 M. Roushani, M. Sarabaegi and A. Rostamzad, *J. Iran. Chem. Soc.*, 2020, **17**, 2407–2413.
142 S. Arif, S. Qudsia, S. Urooj, N. Chaudry, A. Arshad and S. Andleeb, *Biosens. Bioelectron.*, 2015, **65**, 62–70.
143 J. Y. Chen, L. S. Penn and J. Xi, *Biosens. Bioelectron.*, 2018, **99**, 593–602.
144 J. Kankare, *Langmuir*, 2002, **18**, 7092–7094.
145 C. Cheubong, A. Yoshida, Y. Mizukawa, N. Hayakawa, M. Takai, T. Morishita, Y. Kitayama, H. Sunayama and T. Takeuchi, *Anal. Chem.*, 2020, **92**, 6401–6407.
146 S. Tokonami, Y. Nakadoi, M. Takahashi, M. Ikemizu, T. Kadoma, K. Saimatsu, L. Q. Dung, H. Shiigi and T. Nagaoka, *Anal. Chem.*, 2013, **85**, 4925–4929.
147 J. Wang, J. Dai, Y. Xu, X. Dai, Y. Zhang, W. Shi, B. Sellergren and G. Pan, *Small*, 2019, **15**, 1803913.
148 D. L. Robinson, A. Hermans, A. T. Seipel and R. M. Wightman, *Chem. Rev.*, 2008, **108**, 2554–2584.
149 S. Kruss, M. P. Landry, E. Vander Ende, B. M. A. Lima, N. F. Reuel, J. Zhang, J. Nelson, B. Mu, A. Hilmer and M. Strano, *J. Am. Chem. Soc.*, 2014, **136**, 713–724.
150 T. Patriarchi, J. R. Cho, K. Merten, M. W. Howe, A. Marley, W.-H. Xiong, R. W. Folk, G. J. Broussard, R. Liang and M. J. Jang, *Science*, 2018, **360**, eaat4422.
151 B. Kong, A. Zhu, Y. Luo, Y. Tian, Y. Yu and G. Shi, *Angew. Chem., Int. Ed.*, 2011, **50**, 1837–1840.
152 D. Michel, F. Xiao and K. Alameh, *Sens. Actuators, B*, 2017, **246**, 258–261.
153 H. Šípová and J. Homola, *Anal. Chim. Acta*, 2013, **773**, 9–23.

154 K. B. Levin, O. Dym, S. Albeck, S. Magdassi, A. H. Keeble, C. Kleanthous and D. S. Tawfik, *Nat. Struct. Mol. Biol.*, 2009, **16**, 1049–1055.
155 L. Cenci, E. Andreetto, A. Vestri, M. Bovi, M. Barozzi, E. Iacob, M. Busato, A. Castagna, D. Girelli and A. M. Bossi, *J. Nanobiotechnol.*, 2015, **13**, 1–15.
156 A. Garcia-Cruz, O. S. Ahmad, K. Alanazi, E. Piletska and S. A. Piletsky, *Microsyst. Nanoeng.*, 2020, **6**, 1–9.
157 T. Kamra, S. Chaudhary, C. Xu, L. Montelius, J. Schnadt and L. Ye, *J. Colloid Interface Sci.*, 2016, **461**, 1–8.
158 A. L. Campaña, S. L. Florez, M. J. Noguera, O. P. Fuentes, P. Ruiz Puentes, J. C. Cruz and J. F. Osma, *Biosensors*, 2019, **9**, 41.
159 N. L. C. Members, G. L. Myers, R. H. M. Christenson, M. Cushman, C. M. Ballantyne, G. R. Cooper, C. M. Pfeiffer, S. M. Grundy, D. R. Labarthe and D. Levy, *Clin Chem*, 2009, **55**, 378–384.
160 P. S. Jellinger, D. A. Smith, A. E. Mehta, O. Ganda, Y. Handelsman, H. W. Rodbard, M. D. Shepherd, J. A. Seibel, R. Kreisberg and R. Goldberg, *Endocr. Pract.*, 2012, **18**, 1–78.
161 X. Zhang, B. Yao, Q. Hu, Y. Hong, A. Wallace, K. Reynolds, C. Ramsey, A. Maeder, R. Reed and Y. Tang, *Mater. Chem. Front.*, 2020, **4**, 2548–2570.
162 Y. Ma, X.-L. Shen, Q. Zeng, H.-S. Wang and L.-S. Wang, *Talanta*, 2017, **164**, 121–127.
163 X. Xin, S. Sun, M. Wang and R. Jia, *Ionics*, 2020, **26**, 2633–2641.
164 B. Babamiri, A. Salimi and R. Hallaj, *Biosens. Bioelectron.*, 2018, **117**, 332–339.
165 H. Yang, L. Li, Y. Ding, D. Ye, Y. Wang, S. Cui and L. Liao, *Biosens. Bioelectron.*, 2017, **92**, 748–754.
166 M. You, S. Yang, Y. An, F. Zhang and P. He, *J. Electroanal. Chem.*, 2020, **862**, 114017.
167 I. W. Hamley, *Chem. Rev.*, 2012, **112**, 5147–5192.
168 S. Jaiswal, R. Singh, K. Singh, S. Fatma and B. B. Prasad, *Biosens. Bioelectron.*, 2019, **124**, 176–183.
169 M.-A. B. MacKay, M. Kravtsenyuk, R. Thomas, N. D. Mitchell, S. M. Dursun and G. B. Baker, *Front. Psychiatry*, 2019, **10**, DOI: 10.3389/fpsyt.2019.00025.
170 A. Kugimiya and E. Matsuzaki, *Appl. Biochem. Biotechnol.*, 2014, **174**, 2527–2536.
171 M. Yaqoob and A. Nabi, *Talanta*, 2001, **55**, 1181–1186.
172 S. Li, Q. Yu, X. Lu and S. Zhao, *J. Sep. Sci.*, 2009, **32**, 282–287.
173 M. Saha and S. Das, *J. Nanostruct. Chem.*, 2014, **4**, 1–9.
174 A. K. Singh and M. Singh, *J. Electroanal. Chem.*, 2016, **780**, 169–175.
175 M. Roushani, M. Shamsipur and S. M. Pourmortazavi, *J. Appl. Electrochem.*, 2012, **42**, 1005–1011.
176 L. Luo, J. Yang, K. Liang, C. Chen, X. Chen and C. Cai, *Talanta*, 2019, **202**, 21–26.
177 K. He, C. Chen, C. Liang, C. Liu, B. Yang, X. Chen and C. Cai, *Sens. Actuators, B*, 2016, **233**, 607–614.
178 W. Feng, C. Liang, H. Gong and C. Cai, *New J. Chem.*, 2018, **42**, 3503–3508.
179 C. Liang, H. Wang, K. He, C. Chen, X. Chen, H. Gong and C. Cai, *Talanta*, 2016, **160**, 360–366.
180 S. M. Tawfik, M. R. Elmasry, M. Sharipov, S. Azizov, C. H. Lee and Y. I. Lee, *Biosens. Bioelectron.*, 2020, **160**, 112211.
181 G. Zhao, Y. Wang, X. Li, Q. Yue, X. Dong, B. Du, W. Cao and Q. Wei, *Anal. Chem.*, 2019, **91**, 1989–1996.
182 N. Xia, X. Wang, B. Zhou, Y. Wu, W. Mao and L. Liu, *ACS Appl. Mater. Interfaces*, 2016, **8**, 19303–19311.
183 L. Guerrini, R. Arenal, B. Mannini, F. Chiti, R. Pini, P. Matteini and R. A. Alvarez-Puebla, *ACS Appl. Mater. Interfaces*, 2015, **7**, 9420–9428.
184 T. Yang, S. Hong, T. O'Malley, R. A. Sperling, D. M. Walsh and D. J. Selkoe, *Alzheimer's Dement.*, 2013, **9**, 99–112.
185 L. Zhu, J. Zhang, F. Wang, Y. Wang, L. Lu, C. Feng, Z. Xu and W. Zhang, *Biosens. Bioelectron.*, 2016, **78**, 206–212.
186 Y. Yu, L. Zhang, C. Li, X. Sun, D. Tang and G. Shi, *Angew. Chem.*, 2014, **126**, 13046–13049.
187 M. K. Kang, J. Lee, A. H. Nguyen and S. J. Sim, *Biosens. Bioelectron.*, 2015, **72**, 197–204.
188 H.-L. Shuai, X. Wu, K.-J. Huang and Z.-B. Zhai, *Biosens. Bioelectron.*, 2017, **94**, 616–625.
189 L. Liu, F. Zhao, F. Ma, L. Zhang, S. Yang and N. Xia, *Biosens. Bioelectron.*, 2013, **49**, 231–235.
190 F. G. Bellagambi, T. Lomonaco, P. Salvo, F. Vivaldi, M. Hangouët, S. Ghimenti, D. Biagini, F. Di Francesco, R. Fuoco and A. Errachid, *TrAC, Trends Anal. Chem.*, 2020, **124**, 115781.
191 E. Lamy and M. Mau, *J. Proteomics*, 2012, **75**, 4251–4258.
192 C.-K. Yeh, N. J. Christodoulides, P. N. Floriano, C. S. Miller, J. L. Ebersole, S. E. Weigum, J. McDevitt and S. W. Redding, *Tex. Dent. J.*, 2010, **127**, 651.
193 G. Spano, S. Cavalera, F. di Nardo, C. Giovannoli, L. Anfossi and C. Baggiani, *Anal. Methods*, 2019, **11**, 2320–2326.
194 P. Tang, H. Zhang, J. Huo and X. Lin, *Anal. Methods*, 2015, **7**, 7784–7791.
195 A. S. Panchbhai, *J. Oral Maxillofac. Res.*, 2012, **3**, e3.
196 A. Diouf, B. Bouchikhi and N. el Bari, *Mater. Sci. Eng., C*, 2019, **98**, 1196–1209.
197 J. Xu, Q. Sheng, Y. Shen and J. Zheng, *Colloids Surf., A*, 2017, **529**, 113–118.
198 C. Hu, D.-P. Yang, F. Zhu, F. Jiang, S. Shen and J. Zhang, *ACS Appl. Mater. Interfaces*, 2014, **6**, 4170–4178.
199 A. Ciudin, C. Hernández and R. Simó, *Curr. Diabetes Rev.*, 2012, **8**, 48–54.
200 F. Parnianchi, S. Kashanian, M. Nazari, C. Santoro, P. Bollella and K. Varmira, *Microchem. J.*, 2021, **168**, 106367.
201 Ç. Çiçek, F. Yılmaz, E. Özgür, H. Yavuz and A. Denizli, *Chemosensors*, 2016, **4**, 21.
202 C. Song, Y. Li, B. Wang, Y. Hong, C. Xue, Q. Li, E. Shen and D. Cui, *Colloids Surf., B*, 2021, **197**, 111430.
203 W. Xiao, D. Zhi, Q. Pan, Y. Liang, F. Zhou and Z. Chen, *Anal. Methods*, 2020, **12**, 5691–5698.
204 I. Taurino, V. Van Hoof, G. De Micheli and S. Carrara, *Thin Solid Films*, 2013, **548**, 546–550.

205 M. L. Yola, C. Göde and N. Atar, *Electrochim. Acta*, 2017, **246**, 135–140.
206 A.-H. Wu and M.-J. Syu, *Biosens. Bioelectron.*, 2006, **21**, 2345–2353.
207 M.-J. Syu, T.-C. Chiu, C.-Y. Lai and Y.-S. Chang, *Biosens. Bioelectron.*, 2006, **22**, 550–557.
208 C.-Y. Huang, M.-J. Syu, Y.-S. Chang, C.-H. Chang, T.-C. Chou and B.-D. Liu, *Biosens. Bioelectron.*, 2007, **22**, 1694–1699.
209 J. Yang, Y. Hu and Y. Li, *Biosens. Bioelectron.*, 2019, **135**, 224–230.
210 B. B. Prasad, A. Prasad and M. P. Tiwari, *Biosens. Bioelectron.*, 2013, **39**, 236–243.
211 B. B. Prasad and I. Pandey, *Sens. Actuators, B*, 2013, **186**, 407–416.
212 X. Ji, D. Li and H. Li, *Biomed. Chromatogr.*, 2015, **29**, 1280–1289.
213 M. E. Bowers, D. C. Choi and K. J. Ressler, *Physiol. Behav.*, 2012, **107**, 699–710.
214 A. L. LaCrosse and M. Foster Olive, *CNS Neurol. Disord.: Drug Targets*, 2013, **12**, 619–632.
215 P. Luliński, M. Bamburowicz-Klimkowska, M. Dana and D. Maciejewska, *J. Sep. Sci.*, 2017, **40**, 1824–1833.
216 M. Chung, G. Fortunato and N. Radacsi, *J. R. Soc., Interface*, 2019, **16**, 20190217.
217 M. Jia, W. M. Chew, Y. Feinstein, P. Skeath and E. M. Sternberg, *Analyst*, 2016, **141**, 2053–2060.
218 S. M. Mugo and J. Alberkant, *Anal. Bioanal. Chem.*, 2020, **412**, 1825–1833.
219 J. A. Martin, J. L. Chávez, Y. Chushak, R. R. Chapleau, J. Hagen and N. Kelley-Loughnane, *Anal. Bioanal. Chem.*, 2014, **406**, 4637–4647.
220 R. C. Kessler, P. Berglund, O. Demler, R. Jin, K. R. Merikangas and E. E. Walters, *Arch. Gen. Psychiatry*, 2005, **62**, 593–602.
221 N. V. Zaryanov, V. N. Nikitina, E. V. Karpova, E. E. Karyakina and A. A. Karyakin, *Anal. Chem.*, 2017, **89**, 11198–11202.
222 M. Sekar, M. Pandiaraj, S. Bhansali, N. Ponpandian and C. Viswanathan, *Sci. Rep.*, 2019, **9**, 403.
223 K. S. Kim, S. R. Lim, S.-E. Kim, J. Y. Lee, C.-H. Chung, W.-S. Choe and P. J. Yoo, *Sens. Actuators, B*, 2017, **242**, 1121–1128.
224 B. Sun, Y. Gou, Y. Ma, X. Zheng, R. Bai, A. A. A. Abdelmoaty and F. Hu, *Biosens. Bioelectron.*, 2017, **88**, 55–62.
225 W. Tang, L. Yin, J. R. Sempionatto, J. Moon, H. Teymourian and J. Wang, *Adv. Mater.*, 2021, **33**, 2008465.
226 Q. Zhang, D. Jiang, C. Xu, Y. Ge, X. Liu, Q. Wei, L. Huang, X. Ren, C. Wang and Y. Wang, *Sens. Actuators, B*, 2020, **320**, 128325.
227 W. Jia, A. J. Bandodkar, G. Valdés-Ramírez, J. R. Windmiller, Z. Yang, J. Ramírez, G. Chan and J. Wang, *Anal. Chem.*, 2013, **85**, 6553–6560.
228 P. J. Derbyshire, H. Barr, F. Davis and S. P. J. Higson, *J. Physiol. Sci.*, 2012, **62**, 429–440.
229 Z. Stojanovic, J. Erdőssy, K. Keltai, F. W. Scheller and R. E. Gyurcsányi, *Anal. Chim. Acta*, 2017, **977**, 1–9.
230 M.-H. Lee, D. O'Hare, Y.-L. Chen, Y.-C. Chang, C.-H. Yang, B.-D. Liu and H.-Y. Lin, *Biomicrofluidics*, 2014, **8**, 54115.
231 G. Zhang, Y. Yu, M. Guo, B. Lin and L. Zhang, *Sens. Actuators, B*, 2019, **288**, 564–570.
232 C. D. Stehouwer, M. A. Gall, J. W. Twisk, E. Knudsen, J. J. Emeis and H. H. Parving, *Diabetes*, 2002, **51**, 1157–1165.
233 Y.-Z. Wang, D.-Y. Li, X.-W. He, W.-Y. Li and Y.-K. Zhang, *Microchim. Acta*, 2015, **182**, 1465–1472.
234 M. Cieplak, K. Szwabinska, M. Sosnowska, B. K. C. Chandra, P. Borowicz, K. Noworyta, F. D'Souza and W. Kutner, *Biosens. Bioelectron.*, 2015, **74**, 960–966.
235 J. Xia, X. Cao, Z. Wang, M. Yang, F. Zhang, B. Lu, F. Li, L. Xia, Y. Li and Y. Xia, *Sens. Actuators, B*, 2016, **225**, 305–311.
236 X.-T. Ma, X.-W. He, W.-Y. Li and Y.-K. Zhang, *Sens. Actuators, B*, 2017, **246**, 879–886.
237 G. V. Martins, A. C. Marques, E. Fortunato and M. G. F. Sales, *Sens. Bio-Sens. Res.*, 2020, **28**, 100333.
238 H. Jayakody, D. Rowland, C. Pereira, R. Blackwell, T. Lasota, M. Laverick, L. Tisi, H. S. Leese and A. D. S. Walsham, *Sci. Rep.*, 2022, **12**, 1–8.
239 C. H. Hernando, J. A. Á. Serra, M. J. E. Saco, S. Martínez-Nadal and C. V. Cerén, *Anales de Pediatria*, Elsevier, 2020, vol. 93, p. 264.
240 K. Hong, W. Cao, Z. Liu, L. Lin, X. Zhou, Y. Zeng, Y. Wei, L. Chen, X. Liu and Y. Han, *Emerging Microbes Infect.*, 2020, **9**, 2315–2321.
241 A. Wajnberg, M. Mansour, E. Leven, N. M. Bouvier, G. Patel, A. Firpo-Betancourt, R. Mendu, J. Jhang, S. Arinsburg and M. Gitman, *Lancet Microbe*, 2020, **1**, e283–e289.
242 Find©, **https://www.finddx.org/test-directory/**), (accessed March 29, 2022).
243 R. R. X. Lim and A. Bonanni, *TrAC, Trends Anal. Chem.*, 2020, **133**, 116081.
244 G. Seo, G. Lee, M. J. Kim, S.-H. Baek, M. Choi, K. B. Ku, C.-S. Lee, S. Jun, D. Park, H. G. Kim, S.-J. Kim, J.-O. Lee, B. T. Kim, E. C. Park and S. Il Kim, *ACS Nano*, 2020, **14**, 5135–5142.
245 A. G. Ayankojo, R. Boroznjak, J. Reut, A. Öpik and V. Syritski, *Sens. Actuators, B*, 2022, **353**, 131160.
246 Y. Li, Z. Peng, N. J. Holl, M. R. Hassan, J. M. Pappas, C. Wei, O. H. Izadi, Y. Wang, X. Dong and C. Wang, *ACS Omega*, 2021, **6**, 6643–6653.
247 S. Eissa and M. Zourob, *Anal. Chem.*, 2020, **93**, 1826–1833.
248 B. Mojsoska, S. Larsen, D. A. Olsen, J. S. Madsen, I. Brandslund and F. A. Alatraktchi, *Sensors*, 2021, **21**, 390.
249 L. Fabiani, M. Saroglia, G. Galatà, R. de Santis, S. Fillo, V. Luca, G. Faggioni, N. D'Amore, E. Regalbuto and P. Salvatori, *Biosens. Bioelectron.*, 2021, **171**, 112686.
250 A. Raziq, A. Kidakova, R. Boroznjak, J. Reut, A. Öpik and V. Syritski, *Biosens. Bioelectron.*, 2021, **178**, 113029.
251 R. Boroznjak, J. Reut, A. Tretjakov, A. Lomaka, A. Öpik and V. Syritski, *J. Mol. Recognit.*, 2017, **30**, e2635.
252 T. Takeuchi, K. Mori, H. Sunayama, E. Takano, Y. Kitayama, T. Shimizu, Y. Hirose, S. Inubushi, R. Sasaki and H. Tanino, *J. Am. Chem. Soc.*, 2020, **142**, 6617–6624.

253 R. J. Berckmans, R. Lacroix, C. M. Hau, A. Sturk and R. Nieuwland, *J. Extracell. Vesicles*, 2019, **8**, 1688936.
254 S. U. Wang, A. Khan, R. Huang, S. Ye, K. Di, T. Xiong and Z. Li, *Biosens. Bioelectron.*, 2020, **154**, 112056.
255 L. A. Aqrawi, H. K. Galtung, B. Vestad, R. Øvstebø, B. Thiede, S. Rusthen, A. Young, E. M. Guerreiro, T. P. Utheim and X. Chen, *Arthritis Res. Ther.*, 2017, **19**, 1–15.
256 K. Mori, M. Hirase, T. Morishige, E. Takano, H. Sunayama, Y. Kitayama, S. Inubushi, R. Sasaki, M. Yashiro and T. Takeuchi, *Angew. Chem.*, 2019, **131**, 1626–1629.
257 K. Ishihara, T. Ueda and N. Nakabayashi, *Polym. J.*, 1990, **22**, 355–360.
258 H. Im, H. Shao, Y. Il Park, V. M. Peterson, C. M. Castro, R. Weissleder and H. Lee, *Nat. Biotechnol.*, 2014, **32**, 490–495.
259 H. Shao, J. Chung, L. Balaj, A. Charest, D. D. Bigner, B. S. Carter, F. H. Hochberg, X. O. Breakefield, R. Weissleder and H. Lee, *Nat. Med.*, 2012, **18**, 1835–1840.
260 P. Zhang, X. Zhou, M. He, Y. Shang, A. L. Tetlow, A. K. Godwin and Y. Zeng, *Nat. Biomed. Eng.*, 2019, **3**, 438–451.
261 Y. Yoshioka, N. Kosaka, Y. Konishi, H. Ohta, H. Okamoto, H. Sonoda, R. Nonaka, H. Yamamoto, H. Ishii and M. Mori, *Nat. Commun.*, 2014, **5**, 1–8.
262 G. Qiu, A. Thakur, C. Xu, S. Ng, Y. Lee and C. L. Wu, *Adv. Funct. Mater.*, 2019, **29**, 1806761.
263 Y. Zhang, F. Wang, H. Zhang, H. Wang and Y. Liu, *Anal. Chem.*, 2019, **91**, 12100–12107.
264 S. M. Tawfik, M. R. Elmasry, M. Sharipov, S. Azizov, C. H. Lee and Y. I. Lee, *Biosens. Bioelectron.*, 2020, **160**, 112211.
265 H. D. Ertuğrul Uygun, Z. O. Uygun, E. Canbay, N. S. F. Gi Rgi and E. Sezer, *Talanta*, 2020, **206**, 120225.
266 S. P. Usha, A. M. Shrivastav and B. D. Gupta, *Biosens. Bioelectron.*, 2017, **87**, 178–186.
267 Y.-J. Yan, X.-W. He, W.-Y. Li and Y.-K. Zhang, *Biosens. Bioelectron.*, 2017, **91**, 253–261.
268 L. Lin, H.-T. Lian, X.-Y. Sun, Y.-M. Yu and B. Liu, *Anal. Methods*, 2015, **7**, 1387–1394.
269 H. Duan, L. Li, X. Wang, Y. Wang, J. Li and C. Luo, *Spectrochim. Acta, Part A*, 2015, **139**, 374–379.
270 E. N. Primo, M. J. Kogan, H. E. Verdejo, S. Bollo, M. D. Rubianes and G. A. Rivas, *ACS Appl. Mater. Interfaces*, 2018, **10**, 23501–23508.
271 S. Manju, P. R. Hari and K. Sreenivasan, *Biosens. Bioelectron.*, 2010, **26**, 894–897.
272 L. Luo, J. Yang, K. Liang, C. Chen, X. Chen and C. Cai, *Talanta*, 2019, **202**, 21–26.
273 T. Di Giulio, E. Mazzotta and C. Malitesta, *Biosensors*, 2020, **11**, 3.
274 X. Zhang, S. Yang, R. Jiang, L. Sun, S. Pang and A. Luo, *Sens. Actuators, B*, 2018, **254**, 1078–1086.
275 P. Gupta and R. N. Goyal, *RSC Adv.*, 2015, **5**, 40444–40454.
276 R. Keçili, *Int. J. Anal. Chem.*, 2018, **2018**, 4359892.
277 J. Chen, H. Huang, Y. Zeng, H. Tang and L. Li, *Biosens. Bioelectron.*, 2015, **65**, 366–374.
278 S. Wang, G. Sun, Z. Chen, Y. Liang, Q. Zhou, Y. Pan and H. Zhai, *Electrochim. Acta*, 2018, **259**, 893–902.
279 R. Jalili and M. Amjadi, *Sens. Actuators, B*, 2018, **255**, 1072–1078.
280 L. Mergola, S. Scorrano, R. Del Sole, M. R. Lazzoi and G. Vasapollo, *Biosens. Bioelectron.*, 2013, **40**, 336–341.
281 S. P. Ng, G. Qiu, N. Ding, X. Lu and C.-M. L. Wu, *Biosens. Bioelectron.*, 2017, **89**, 468–476.
282 H. Hai, X. An and J. Li, *Anal. Methods*, 2015, **7**, 2210–2214.
283 X. Wang, J. Yu, J. Li, Q. Kang, D. Shen and L. Chen, *Sens. Actuators, B*, 2018, **255**, 268–274.
284 S. E. Diltemiz and O. Uslu, *Biotechnol. Prog.*, 2015, **31**, 55–61.
285 P. Luliński, M. Bamburowicz-Klimkowska, M. Dana and D. Maciejewska, *J. Sep. Sci.*, 2017, **40**, 1824–1833.
286 Y. Tian, P. Deng, Y. Wu, Z. Ding, G. Li, J. Liu and Q. He, *Biomolecules*, 2019, **9**, 294.
287 W. Zheng, M. Zhao, W. Liu, S. Yu, L. Niu, G. Li, H. Li and W. Liu, *J. Electroanal. Chem.*, 2018, **813**, 75–82.
288 A. Göçenoğlu Sarıkaya, B. Osman, T. Çam and A. Denizli, *Sens. Actuators, B*, 2017, **251**, 763–772.
289 V. Ricotta, Y. Yu, N. Clayton, Y.-C. Chuang, Y. Wang, S. Mueller, K. Levon, M. Simon and M. Rafailovich, *Analyst*, 2019, **144**, 4266–4280.
290 L. A. Agrofoglio, A. Krstulja, C. De Schutter, P. Favetta, R. Delépée, V. Roy, C. Dejous, H. Hallil, J.-L. Lachaud and N. Lebal, *IRBM*, 2014, **35**, 66–71.
291 MIP Technologies, **http://www.miptechnologies.com/**, (accessed March 29, 2022).
292 Allergy Amulet, **https://www.allergyamulet.com/**, (accessed May 29, 2022).
293 M. Sundhoro, S. R. Agnihotra, B. Amberger, K. Augustus, N. D. Khan, A. Barnes, J. BelBruno and L. Mendecki, *Food Chem.*, 2021, **344**, 128648.
294 R. Rapini, F. Canfarotta, E. Mazzotta, C. Malitesta, G. Marrazza, S. Piletsky and E. Piletska, *Analyst*, 2019, **144**, 7290–7295.
295 MIP Diagnostics, **https://www.mip-dx.com/**, (accessed March 29, 2022).
296 Z. Altintas, A. Guerreiro, S. A. Piletsky and I. E. Tothill, *Sens. Actuators, B*, 2015, **213**, 305–313.
297 K. Smolinska-Kempisty, A. Guerreiro, J. Czulak and S. Piletsky, *Sens. Actuators, B*, 2019, **301**, 126967.
298 MarketsandMarkets™, **https://www.marketsandmarkets.com/Market-Reports/biosensors-market-798.html**, (accessed March 29, 2022).